Glucocorticoid receptor and RUNX transcription factors cooperatively drive CD8 T cell dysfunction in human cancer

Christopher J Ward[1$], Soura Chakraborty[1$], Sanu K Shaji[1], Clara Veiga-Villauriz[1], Aws Al-deka[1], Qiuchen Zhao[1], Jhuma Pramanik[1], Xi Chen[2] and Bidesh Mahata[1*]

1. Department of Pathology, University of Cambridge, Cambridge, CB2 1QP, UK

2. Shenzhen Key Laboratory of Gene Regulation and Systems Biology, Department of Biology, School of Life Sciences, Southern University of Science and Technology, Shenzhen, China

[$] Equal contribution

*To whom correspondence should be addressed: bm562@cam.ac.uk

Abstract

Glucocorticoids (GCs) are potent modulators of immune responses; however, the mechanisms by which GCs regulate gene expression in human CD8 T cells remain incompletely defined. Here, we delineate how physiological cortisol signalling shapes the transcriptional and chromatin landscapes of primary human CD8 T cells. We identify a substantial cohort of GC-responsive genes that are co-regulated through the cooperative activity of the glucocorticoid receptor (GR) and RUNX transcription factors. Integrative RNA sequencing and ChIP sequencing analyses identified genome-wide cortisol-responsive immunoregulatory genes. Genetic deletion of the GR (encoded by *NR3C1*) abolished cortisol-induced gene expression changes, confirming GR-dependency. Notably, GR chromatin occupancy in cortisol-treated CD8 T cells was strongly enriched at RUNX transcription factor (TF) motif rather than canonical GC response elements (GREs). Co-immunoprecipitation assays validated a ligand-dependent physical interaction between GR and RUNX and revealed the interacting domains. Single-cell transcriptomic analyses of tumour infiltrating CD8 T cells revealed significant enrichment of cortisol-responsive genes, indicating an active GC signalling (response) within the tumour microenvironment. GR-RUNX dual controlled genes were enriched in tumour-infiltrating CD8 T cells across multiple cancer types, including lung adenocarcinoma, head and neck squamous carcinoma, pancreatic cancer, and breast cancer. We found GR-RUNX co-regulated genes are predominantly expressed in the predysfunctional state of CD8 T cell population of different solid tumours. These results suggest that local cortisol signalling within tumour microenvironments drives CD8 T cell dysfunction through GR-RUNX TF cooperation. Collectively, our findings identify RUNX3 TF as a critical mediator of GR signalling in human CD8 T cells and reveal a novel mechanism by which endogenous GCs influence antitumour immunity, which could be therapeutically targetable.

Introduction

Glucocorticoids (GCs) are steroid hormones widely recognised for their potent immunomodulatory and anti-inflammatory properties. Synthetic GCs, such as dexamethasone, betamethasone and prednisone, are extensively utilised in clinical settings to treat autoimmune disorders, inflammatory diseases, and haematological malignancies due to their ability to suppress immune cell activation and cytokine production[1,2]. Endogenous GCs, primarily cortisol in humans, also play critical roles in regulating immune homeostasis and responses under physiological and stress conditions[3]. Chronic or dysregulated GC signalling has been implicated in impaired antitumour immunity and cancer progression[2,4,5-10]. Despite extensive studies on synthetic GC-mediated immunosuppression, the precise molecular mechanisms by which physiological cortisol signalling modulates human CD8 T cell functions, particularly within tumour microenvironments, remain incompletely understood.

The GC receptor (GR), encoded by the *NR3C1* gene, is a ligand-activated transcription factor belonging to the nuclear receptor superfamily. Upon ligand binding, GR translocates into the nucleus, binds chromatin at GC response elements (GREs), and regulates target gene expression through direct DNA binding or tethering interactions with other transcription factors[11]. Although classical GRE-dependent mechanisms have been extensively characterised in various cell types, emerging evidence suggests that GR can also regulate gene expression through interactions with non-canonical transcriptional partners. GR can modulate gene expression in immune cells through protein–protein interactions with other transcription factors such as NF-κB and AP-1[12]. This “tethering” or “composite” model of gene regulation allows GR to repress or activate a distinct subset of genes indirectly, without binding DNA at traditional GRE motifs. For example, GR can bind to NF-κB p65 subunits, preventing NF-κB from inducing proinflammatory cytokine transcription. Conversely, it can cooperate with AP-1 to enhance the expression of anti-inflammatory mediators. Such interactions enable GR to modulate gene expression programs in a highly context-dependent manner[13,14]. Identification of these non-canonical GR partners in specific immune subsets is crucial for understanding the complex regulatory networks orchestrated by GCs in a physiological or pathological context of immune regulation.

CD8 T cells are central players in adaptive immunity, mediating cytotoxic responses against infected cells (such as virus infected) or cancer cells. Effective CD8 T cell responses are critical for tumour control and elimination. However, persistent antigen exposure and immunosuppressive signals within tumour microenvironments frequently drive CD8 T cell dysfunction or exhaustion, limiting their antitumour efficacy[15,16]. In the context of CD8 T cells,

GCs have been shown to suppress T cell effector programmes, including the upregulation of checkpoint inhibitory proteins (CTLA-4, PD-1, LAG-3, TIM3) in a context dependent manner[5,17,18]. Recent studies indicate that the local GC signalling may contribute significantly to immune suppression within tumour microenvironment by promoting T cell dysfunction[2,4,5-7], yet the underlying transcriptional mechanisms remain largely unexplored.

RUNX transcription factors represent a family of evolutionarily conserved proteins crucially involved in lineage specification, differentiation, proliferation, and functional regulation of various immune cell subsets[19]. RUNX proteins (all three paralogues RUNX1-3) bind DNA through conserved Runt domains (>95% sequence identity) at core consensus motif YGYGGTY to regulate gene expression programs essential for hematopoietic development and immune function. Among the RUNX family members (RUNX1-3), RUNX2 is predominantly known for its roles in osteogenesis. However, recent evidence reveals its broader involvement in immune regulation and cancer biology[20]. RUNX1 and RUNX3 are critical regulators of CD8 T cell development and function. During thymopoiesis, they collaborate to repress CD4 and enforce CD8 lineage commitment[21,22]. In mature CD8 cytotoxic T lymphocytes (CTLs), RUNX3 dominates. It directly binds to the enhancers (e.g., *Cd8a* enhancer E8I) to maintain CD8 expression[21,22] and activating effector genes like *Ifng, Gzmb* (granzyme B), and *Prf1* (perforin) [21,22]. Runx3 deficiency severely impairs cytolytic activity and proliferation[21,22], while also promoting tissue-resident memory (T_{RM}) CD8 T cells by upregulating tissue-retention genes and suppressing recirculation[23]. Runx1 supports thymocyte transitions and mature T cell homeostasis but plays a secondary role in peripheral CTLs[24]. Runx2, though largely restricted to early thymic development, contributes to CD8 memory cell maintenance[1,23]. Together, Runx3 emerges as the central driver of CD8 T cell identity, effector function, and tissue residency, while Runx1 and Runx2 provide developmental and memory-related support. The potential interaction between GR signalling and RUNX transcription factors in CD8 T cells has not been previously investigated.

In this study, we aimed to elucidate how physiological cortisol signalling modulates human CD8 T cell function at the molecular level. Using integrative RNA sequencing (RNA-seq) and ChIP sequencing (ChIP-seq) approaches combined with genetic deletion and biochemical validations, we demonstrate that cortisol profoundly reshapes the transcriptional landscape of primary human CD8 T cells through ligand-dependent GR-RUNX cooperation. We further provide single-cell transcriptomic evidence that this novel GR-RUNX regulatory axis operates within tumour-infiltrating CD8 T cells across multiple cancer types. Our findings identify RUNX as a critical non-canonical partner of GR in human CD8 T cells and suggest a previously unrecognised mechanism by which local endogenous GC signalling within tumour influence

antitumour immunity, offering new therapeutic opportunities aimed at enhancing cancer immunotherapy efficacy by targeting context-specific GR interactions.

Results

Cortisol reshapes the transcriptional landscape and signalling pathways in human activated CD8 T cells

To investigate how physiological cortisol influences the transcriptional profile of human CD8 T cells, we performed RNA-seq on *in vitro* activated primary CD8 T cells treated with cortisol (100 nM, 48 hours) or vehicle control (Figure 1a). Differential gene expression analysis identified 297 significantly regulated genes (169 upregulated, 128 downregulated) (Figure 1b). Among the most strongly induced genes were *TSC22D3, IL7R, FKBP5 and PIK3IP1*. Notably, *PIK3IP1,* a negative regulator of PI3Ks, *and* amphiregulin (*AREG*), a cytokine implicated in tissue repair and immunosuppression, emerged as a novel cortisol-induced gene in CD8 T cells. A complete list of these differentially expressed genes can be accessed in the Supplementary Table S1. Gene set enrichment analysis (GSEA) using the Hallmark gene set collection revealed distinct patterns of pathway regulation following GC treatment (Figure 1c, Supplementary Table S2). Cortisol treatment enriched gene sets associated with cell cycle control and metabolic regulation including E2F targets, MYC targets, G2M checkpoint, and mTORC1 signalling. Conversely, inflammatory and effector-associated programmes were significantly supressed including inflammatory response, TNFα signalling via NF-κB, IL6/JAK/STAT3 signalling, apoptosis, and IL2/STAT5 signalling. These data suggest cortisol enforces a metabolic checkpoint state in CD8 T cells, limiting inflammatory effector functions while simultaneously promoting cell survival and proliferation-associated pathways.

To confirm GR-dependency of these transcriptional changes, we employed CRISPR-Cas9-mediated knockout of the GR (*NR3C1*) in primary human CD8 T cells (Fig 1d). Loss of GR expression abolished cortisol-induced upregulation of target genes (e.g., *TSC22D3*, *IL7R, FKBP5, PIK3IP1 and AREG*), confirming direct GR involvement in mediating cortisol-driven transcriptional reprogramming (Figure 1e). A complete list of differentially expressed genes in *NR3C1* knocked out CD8 T cell can be found in Supplementary Table S1.

In CD8 T cells, these 122 genes get upregulated in hydrocortisone (cortisol) treatment but downregulated when the GR (*NR3C1*) is knocked out. The Venn diagram analysis demonstrated that 47 genes were exclusively upregulated by cortisol in a GR-independent manner (Mock HC vs. Vehicle), while 54 genes were uniquely upregulated in GR-KO cells independent of the ligand cortisol (Figure 1f). 122 genes were upregulated in both conditions,

147 suggesting GR-dependent mechanisms of cortisol-induced gene activation. Similarly, we
148 found 84 genes get downregulated in cortisol treated CD8 T cell and get upregulated in *NR3C1*
149 KO CD8 T cells. These findings identify cortisol induced true upregulated and downregulated
150 genes in CD8 T cells. These findings also indicate that while a substantial proportion of
151 cortisol-regulated genes require functional GR signalling, a subset of genes is expressed in a
152 cortisol or GR-independent mechanisms.
153
154 To gain further insight into the functional implications of all cortisol-responsive genes
155 (including both GR-dependent and GR-nondependent genes), we examined differentially
156 expressed transcription factors and various receptors (Figure 1g). The heatmap analysis
157 revealed distinct expression patterns of transcription factors regulated by cortisol treatment in
158 both GR-sufficient and GR-deficient conditions. Several transcription factors, including
159 *ZBTB16, ELK3, TSC22D3, VDR and CEBPB*, showed pronounced regulation following
160 cortisol treatment. The receptor expression analysis identified multiple classes of differentially
161 expressed receptors, including cytokine receptors (e.g., *IL10RA, CCR7, IL7R, CXCR4*),
162 transporters (e.g., *SLC3A2, SLC1A5*), cell surface and adhesion receptors (e.g., *PTGIR,*
163 *ITGB2, ADGRG5*). Among these, several interleukin receptors showed predominantly GR-
164 dependent regulation, while others exhibited mixed patterns of GR-dependent and
165 independent expression changes. These findings highlight the complex interplay between GR-
166 dependent and independent mechanisms in mediating the effects of cortisol on the
167 transcriptional landscape of CD8 T cells, with potential implications for understanding GC
168 actions on immune function.
169
170 Together, these results demonstrate that physiological cortisol reshapes the transcriptional
171 landscape of human CD8 T cells through GR-dependent regulation of immunomodulatory
172 genes and pathways, highlighting a novel role for GCs in controlling T cell functionality via
173 metabolic checkpoint enforcement.
174
175 **Genome-wide chromatin occupancy reveals the direct target genes of GR and its**
176 **noncanonical association with RUNX transcription factors**
177 To elucidate the molecular mechanisms underlying cortisol-mediated transcriptional
178 reprogramming in activated CD8 T cells, we performed chromatin immunoprecipitation
179 followed by sequencing (ChIP-seq) to map genome-wide GR binding sites upon cortisol
180 treatment. Primary human CD8 T cells from healthy donors were activated *in vitro* and treated
181 with cortisol (100 nM, 48 hours) or vehicle (Figure 2a). GR-bound chromatin regions were
182 identified by ChIP-seq. Cortisol elicited a robust GR chromatin-binding response, yielding
183 4,871 high-confidence GR peaks relative to vehicle controls (Figure 2b; Supplementary Table

184 S3). Motif enrichment analysis of these GR-bound genomic regions surprisingly revealed no
185 significant enrichment of canonical GREs, however, showed a striking enrichment of non-
186 canonical enrichment of RUNX transcription factor binding motifs upon cortisol treatment
187 (Figure 2b). Specifically, RUNX motifs were present in approximately 12.6% (Donor A) and
188 35.92% (Donor B) of GR-bound peaks in cortisol-treated cells. Other transcription factor motifs
189 such as TEAD and NFAT also showed modest enrichment following cortisol stimulation
190 (Figure 2b). These data suggest that cortisol-induced GR chromatin occupancy in CD8 T cells
191 preferentially occurs at genomic loci harbouring non-canonical binding to other TFs sites,
192 particularly RUNX binding sites rather than canonical GREs. However, we observed donor-
193 to-donor variability. Cross-donor comparison of Donor A and Donor B ChIP-seq analysis of
194 CD8 T cell identifies 1103 common peaks between donors CD8 T cells treated with
195 hydrocortisone (cortisol) (Figure 2c). Despite the donor-to-donor variability, 344 overlapped
196 peaks were detected between vehicle-treated and hydrocortisone (cortisol) treated samples
197 (Figure 2d). It indicates extensive cortisol-dependent remodelling of GR occupancy in CD8 T
198 cells. We identified 81 putative direct targets of GC by integrating GR-occupied genomic
199 regions from ChIP-seq and cortisol-induced upregulated genes (Figure 2e). We also
200 observed, 50 of these 81 target genes were associated with GR peaks containing RUNX motif,
201 revealed their coregulation by GR-RUNX interaction. (Figure 2f). Notably, this gene set
202 included critical immunoregulatory targets induced by cortisol such as *TSC22D3, IL7R,*
203 *FKBP5 and PIK3IP1* (Figure 2g). Further genomic annotation analysis indicated that cortisol-
204 induced GR binding predominantly localised to intronic (31%) and promoter-proximal regions
205 (31%), supporting a regulatory network distinct from classical GRE driven enhancer
206 occupancy. (Supplementary figure S1a). Collectively, these data implicate RUNX-associated
207 chromatin engagement as dominant feature of GR-dependent gene regulation in activated
208 CD8 T cell. The list of GR direct target genes can be found in Supplementary Table S4.
209
210 **Ligand-dependent interaction between GR and RUNX3 orchestrates cortisol-induced**
211 **gene regulation in CD8 T cells**
212 Given the prominent enrichment of RUNX motifs at GR-bound genomic regions (Figure 2), we
213 hypothesised that GR might physically interact with RUNX transcription factors in a ligand-
214 dependent manner. To test this hypothesis, first we compared the expression level of RUNX
215 transcription factor in human CD8 T cells and found RUNX3 is predominantly expressed
216 (Supplementary figure S1b). We therefore tested whether GR can physically interact with
217 RUNX3 upon GC stimulation. We performed co-immunoprecipitation (co-IP) experiments in
218 HEK293T cells transiently expressing GR and RUNX3 in the presence or absence of cortisol
219 stimulation (100 nM, 36 hours) (Figure 3a). To define interacting domains of RUNX3 and GR
220 for this GR-RUNX3 interaction, based on the previous research, we deleted specific domains

221 of GR (NR3C1) and RUNX3 (Figure 3b)[25,26]. We observed GR and RUNX3 physically interact
222 (Figure 3c). Removal of the GR N-terminal AF1 transactivation region (ΔAF1-NR3C1)
223 substantially diminished RUNX co-precipitation compared with WT GR, indicating that the
224 AF1-containing N-terminus contributes critically to stable GR–RUNX complex formation
225 (Figure 3c). Conversely, deletion of the RUNX3 transactivation and inhibitory regions (ΔTAD
226 ID-RUNX3) also weakened the interaction between RUNX3 and GR, demonstrating that
227 RUNX3 C-terminal regulatory domains are required for efficient association with GR (Figure
228 3c). ΔTAD RUNX3 deletion mutation was not enough to diminish this interaction (Figure 3c).
229 This co-IP analysis also demonstrated that RUNX3 co-precipitated with GR only upon cortisol
230 treatment, confirming ligand-dependent formation of a GR-RUNX3 protein complex (Figure
231 3c).
232
233 To assess the functional relevance of this interaction in primary CD8 T cells, we integrated
234 our GR ChIP-seq, RNA-seq with previously publicly available RUNX target genes datasets
235 that were reported based on RUNX ChIP-seq and RNA-seq. Integrating cortisol-responsive
236 genes containing proximal GR peaks enriched for RUNX motifs with RUNX1 target genes
237 identified 12 genes that showed strong cortisol induction together with nearby GR–RUNX motif
238 occupancy, consistent with direct co-regulation by GR and RUNX transcription factors
239 (Supplementary figure S1c). Next, we performed analogous integration with RUNX2 target
240 genes and stratified the genes that are upregulated (45 genes) or downregulated (7 genes)
241 by the cortisol induced GR-RUNX complex (Supplementary figure S1d). Using RUNX3
242 focused gene set integration in CD8 T cell, we observed 41 genes co-upregulated by GR-
243 RUNX3 and 5 genes co-downregulated by GR-RUNX3 axis (Figure 3d). All the gene names
244 corresponding to this figure have been listed in supplementary Table S5.
245
246 Collectively, these results demonstrate a model in which cortisol promotes physical interaction
247 and functionally transcriptional cooperation between GR and RUNX3 in CD8 T cell. This
248 ligand-dependent GR-RUNX interaction expands the regulatory repertoire of GCs beyond
249 classical GRE-mediated transcriptional control, highlighting a previously unrecognised
250 molecular mechanism by which endogenous GCs modulate human CD8 T cell function.
251
252 **GR-dependent cortisol-induced gene signature is enriched in tumour-infiltrating CD8 T**
253 **cells across multiple cancer types**
254 Given our findings that cortisol signalling profoundly reshapes the transcriptional landscape of
255 human CD8 T cells via GR-RUNX cooperation, we next explored whether this regulatory axis
256 is relevant in the tumour microenvironment. To address this, we reanalysed publicly available
257 single-cell scRNA-seq datasets from tumour-infiltrating lymphocytes derived from patients

258 with breast cancer (Figure 4a), lung adenocarcinoma (Figure 4b), head and neck squamous
259 cell carcinoma (HNSCC) (Figure 4c) and pancreatic adenocarcinoma (Figure 4d). We scored
260 steroid responsiveness in tumour infiltrating CD8 T cell and matched blood derived or matched
261 tissue resident CD8 T cells based on the cortisol-responsive gene signature identified in our
262 primary human CD8 T cell model (including key genes such as *TSC22D3, IL7R, FKBP5,*
263 *PIK3IP1* and *AREG*. Strikingly, single-cell transcriptomic analyses revealed a consistent and
264 significant enrichment of cortisol-induced genes in tumour-infiltrating CD8 T cells across all
265 four cancer types examined (Figure 4a-d), suggesting potential heightened responsiveness to
266 local GC cues.
267
268 These observations indicate that endogenous GC signalling actively operates within tumour
269 microenvironments to modulate CD8 T cell function, potentially contributing to an
270 immunosuppressive state that favours tumour immune evasion. Collectively, these findings
271 underscore the clinical relevance of GR-mediated transcriptional regulation in shaping
272 immune responses within tumours and highlight the potential therapeutic value of targeting
273 GR to reinvigorate antitumour immunity.
274
275 **Elevated expression of RUNX-GR co-regulated genes in tumour-infiltrating CD8 T cells**
276 **across cancer types**
277 We next investigated the expression patterns and functional significance of RUNX-GR co-
278 regulated genes in CD8 T cells across multiple cancer types. We derived a unified
279 transcriptional readout of GR–RUNX cooperation. Specifically, we integrated GR–RUNX1-,
280 GR–RUNX2- and GR–RUNX3-mediated upregulated gene sets (12, 45 and 41 genes,
281 respectively from Supplementary figure S1, Figure 3d) and identified a shared 50-gene core
282 signature. Publicly available single-cell transcriptomic datasets of CD8 T cells isolated from
283 tumours and matched adjacent normal tissue or blood across four major malignancies: triple-
284 negative breast cancer (TNBC), lung cancer, head and neck squamous cell carcinoma
285 (HNSC), and pancreatic ductal adenocarcinoma (PDAC) were reanalysed (Figure 5a-d).
286 Across all datasets, RUNX-GR co-regulated genes exhibited significantly elevated expression
287 in tumour-infiltrating CD8 T cells compared to their non-tumour counterparts (Figure 5a-d).
288 The dot plots both the fraction of the cells expressing each gene (dot size) and average
289 expression level (colour intensity) were consistently increased in tumour infiltrating CD8 T cell
290 population in these cancer types indicating broad activation of RUNX-GR programme within
291 the tumour microenvironment.
292
293 To assess the functional relevance of this expression pattern, we calculated per-cell module
294 scores using AddModuleScore method (Figure 5e-h). Higher module scores, indicative of

elevated RUNX-GR co-regulated gene expression, strongly correlated with increased expression of established T cell exhaustion/dysfunction markers. This correlation was consistent across TNBC (Figure 5e), lung cancer (Figure 5f), HNSC (Figure 5g) and PDAC (Figure 5h), highlighting a conserved link between RUNX-GR transcriptional activity and the exhausted phenotype in tumour-infiltrating CD8 T cells. These findings indicate that RUNX-GR dependent gene regulation is particularly prominent within the tumour microenvironment, suggesting its potential role in shaping the tumour-infiltrating CD8 T cells dysfunction In reanalysed single-cell RNA-seq datasets of tumour-infiltrating CD8 T cells from TNBC, lung cancer, HNSC and PDAC, we classified CD8 T cells into naïve-like, cytotoxic, pre-dysfunctional and dysfunctional states using established marker-gene signatures[27]. When the GR–RUNX co-regulated gene module was overlaid onto the same UMAP embeddings, cytotoxic CD8 T cells consistently formed a spatially distinct cluster from cells with high GR–RUNX module expression. Instead, GR–RUNX target-gene expression preferentially localised to regions enriched for the pre-dysfunctional programme and was partially adjacent to dysfunctional states, consistent with an association between GR–RUNX cooperation and acquisition of dysfunction in tumour-infiltrating CD8 T cells (Figure 6a-d).

Single-cell trajectory analysis reveals an association between cortisol-responsive gene expression and CD8 T cell dysfunction in cancer

To investigate how cortisol signalling affects CD8 T cell differentiation within the tumour microenvironment, we performed single-cell trajectory inference analysis on CD8 T cells isolated from lung tumours and paired peripheral blood samples from patients with lung cancer. Using the Monocle algorithm, pseudo-temporal trajectories were constructed based on single-cell transcriptomic profiles (Supplementary figure S2a). Cells expressing high levels of cortisol-responsive genes (*TSC22D3, IL7R, FKBP5*) were predominantly positioned along trajectory branches associated with progression towards terminal exhaustion or dysfunction, characterised by increased expression of inhibitory receptors, such as *PDCD1, CTLA4, HAVCR2, TIGIT, LAYN, and TOX* (Supplementary figure S2b). In contrast, cells exhibiting lower cortisol-responsive gene signatures were primarily associated with early activation states. These results suggest that GC signalling within the tumour microenvironment is activated shortly after CD8 T cells infiltrate the tumour, potentially driving them toward dysfunctional differentiation states.

Discussion

GC signalling in T cells is context and dose-dependent, with endogenous GCs playing both immunoenhancing and immunosuppressive roles[28]. Under physiological conditions, circadian GC elevations promote CD8 T cell trafficking, survival, and activation[29], while perinatal

332 exposure programs long-term CD8 T cell immunity[30]. However, sustained or excessive GC
333 exposure—as occurs via local extra-adrenal steroid biosynthesis within tumour
334 microenvironments[5]—drives the pathological CD8 T cell dysfunction we describe here.
335
336 In this study, we reveal that physiological cortisol signalling fundamentally remodels the
337 transcriptional and chromatin landscapes of human CD8 T cells through a previously
338 unrecognised, ligand-dependent cooperation between the GR and RUNX transcription
339 factors. By integrating RNA sequencing, ChIP sequencing, genetic perturbation, biochemical
340 validation, and single-cell transcriptomic analyses of tumour-infiltrating lymphocytes, we
341 identify a novel GR-RUNX regulatory axis that significantly modulates CD8 T cell function
342 within the tumour microenvironment.
343
344 Our findings extend the current understanding of GR biology, demonstrating that GR can
345 regulate gene expression via non-canonical interactions with RUNX transcription factors,
346 rather than exclusively through classical GREs. Traditionally, GR-mediated transcriptional
347 regulation has been attributed to direct DNA binding at GREs or through tethered interactions
348 with factors such as NF-κB and AP-1[1,11]. Here, we provide evidence that, in cortisol-treated
349 human CD8 T cells, GR preferentially occupies genomic regions enriched for RUNX motifs.
350 Co-immunoprecipitation experiments confirm a direct, ligand-dependent interaction between
351 GR and RUNX3, positioning RUNX3 as a critical non-canonical partner that enables GR to
352 access distinct regulatory regions beyond those governed by classical GRE-driven
353 mechanisms. We observed cortisol promotes the interaction between GR and RUNX3. We
354 also observed that AF1 region of NR3C1 and C-terminal TAD/ID region of RUNX3 are
355 required for efficient complex formation. Notably, GR disruption did not significantly alter a
356 subset of cortisol-responsive genes, indicating that cortisol can reshape CD8 T cell
357 transcription through GR-independent mechanism. This is consistent with cortisol may act as
358 a broad cellular stimulus that can elicit rapid non-genomic signalling (second-messenger
359 pathway) and activate downstream transcription factors, or CD8 T cell may use alternate
360 cortisol-sensing and metabolic pathways under long-term cortisol exposure. However, this
361 GR-independent component was distinct from GR-RUNX coregulated module.
362
363 RUNX transcription factors are established regulators of immune cell differentiation and
364 function[19]. Our data uncover an unexpected role for RUNX3 in human CD8 T cells as a pivotal
365 mediator of cortisol-induced immunomodulation. Genetic ablation of GR expression abolishes
366 cortisol-induced gene expression changes, confirming direct GR dependency. Moreover,
367 cortisol-induced genes with proximal GR-RUNX motif occupancy include key

immunoregulatory factors such as *IL7R, FKBP5, TSC22D3, PIK3IP1* and *AREG*, implicating RUNX as a crucial determinant of GC-driven immunomodulation.

A particularly intriguing observation from our study is the paradoxical regulation of signalling pathways by cortisol in CD8 T cells. Cortisol robustly suppressed inflammatory pathways (e.g., TNF-α/NF-κB and IL-2/STAT5 signalling) while simultaneously activating pathways associated with cell survival and proliferation (mTORC1 signalling, G2/M checkpoint). This dual regulatory pattern suggests that cortisol enforces a metabolic checkpoint state, limiting inflammatory effector functions while maintaining viability and proliferative capacity. Such metabolic reprogramming may facilitate prolonged persistence of dysfunctional or exhausted T cells within tumours rather than productive effector differentiation, thus contributing to impaired antitumour immunity. An important question for future work is whether GR-RUNX co-operation preferentially supports maintenance of dysfunctional states, entry into exhaustion trajectories or both and how this is influenced by antigen load, co-stimulation and cytokines in the tumour microenvironment.

Our findings reveal that RUNX-GR dependent gene regulation is particularly prominent within the tumour microenvironment across multiple cancer types. This tumour-specific upregulation suggests that local factors within the tumour might be driving this regulatory programme. Local steroid biosynthesis within the tumour microenvironment[5,6,9] provides sustained cortisol exposure inducing the GC signalling pathway, which subsequently activates RUNX-GR-mediated transcriptional programs that influence the fate and function of tumour-infiltrating CD8 T cells. The co-regulation by RUNX factors and GR in tumour-infiltrating T cells is particularly intriguing given that both transcription factor families have been implicated in immune cell differentiation and function. RUNX family transcription factors are known to function redundantly, with RUNX1, RUNX2, and RUNX3 often binding to the same genomic sites and collaboratively regulating similar target genes. GR collaborates with pioneer factors and other transcription factors to regulate target gene expression[31-34]. Here we identify RUNX3 as a critical GR co-factor to regulate cell type-specific transcriptional programs. The observed correlation between RUNX-GR co-regulated gene expression and T cell exhaustion markers suggests that this transcriptional program may contribute to the development of the exhausted phenotype that characterises many tumour-infiltrating T cells. In tumour-infiltrating CD8 T cell subsets we observed GR–RUNX target-gene expressing cells were transcriptionally aligned with pre-dysfunctional state and were distinct from cytotoxic CD8 T cell cluster. Conceptually, this observation supports a model in which cortisol signalling through GR-RUNX modulation reinforces the establishment of an intermediate pre-dysfunctional state that can lead to an exhausted phenotype. However detailed molecular mechanism needs further exploration.

This finding provides new insights into the molecular mechanisms that may underlie T cell dysfunction within the tumour microenvironment and identifies potential therapeutic targets for enhancing anti-tumour immunity. Genetic disruption of RUNX3 in peripheral or tumour-infiltrating CD8 T cell and studying its effects in anti-tumour cytotoxicity in cortisol rich microenvironment will elucidate the mechanism of GR-RUNX mediated CD8 T cell dysfunction. Indeed, recent studies have highlighted local GC production within tumours as an immunosuppressive mechanism exploited by cancer cells to evade immune surveillance[2,5-8,35-39]. Our results provide mechanistic insights into how this local steroid signalling axis may operate at the transcriptional level through GR-RUNX cooperation leading T cell dysfunction.

From a translational perspective, our findings suggest novel therapeutic opportunities aimed at improving cancer immunotherapy efficacy by targeting context-specific GR interactions. Systemic inhibition of GC signalling is challenging as GC maintains physiological homeostasis; thus, selective disruption of GR-RUNX3 interactions or downstream targets identified herein may represent promising therapeutic strategies to enhance antitumour immunity without broadly compromising physiological GC functions. Future studies should explore small-molecule inhibitors or targeted genetic approaches to specifically disrupt GR-RUNX3 interactions in preclinical tumour models. Exploring downstream effectors of RUNX-GR module can reveal new druggable targets to enhance anti-tumour immunity.

In conclusion, our study identifies RUNX3 as a novel non-canonical partner of GR in human CD8 T cells and reveals a previously unrecognised mechanism by which endogenous GCs modulate antitumour immunity. Targeting context-specific transcription factor interactions represents an exciting new avenue for therapeutic intervention aimed at reversing steroid-driven immunosuppression within tumours.

Limitations of the study

Nevertheless, several questions remain unanswered: First, although we demonstrated robust ligand-dependent GR-RUNX3 interaction *in vitro* and identified direct target genes through integrative genomic analyses, further studies are required to clarify the precise molecular determinants mediating this interaction at endogenous loci and its functional outcome changing chromatin structure at the endogenous locus. Second, additional research is needed to delineate the relative contributions of RUNX family members in mediating GC responses in distinct immunological contexts. Finally, future work should validate our findings using *in vivo* tumour models to assess whether disrupting GR-RUNX interactions can effectively restore CD8 T cell functionality and enhance antitumour responses.

Methods

Human CD8 T cell culture

Peripheral blood samples from healthy male adult donors (n=3) were obtained by informed consent. Peripheral blood mononuclear cells (PBMCs) were recovered through density gradient centrifugation using Ficoll-Paque Plus (GE Healthcare). CD8 T cells were isolated from PBMCs. CD8 T cells were isolated from PBMCs by immunomagnetic negative selection (Stem Cell Technologies). CD8 T cells were cultured for a total of 8 days in Immunocult-XF T Cell Expansion media (Stem Cell Technologies) with 50 µg/mL of Gentamicin (Gibco). Isolated cells were stimulated with plate bound anti-CD3 (Biolegend, Clone: OKT3, 1 µg/mL) and anti-CD28 (Biolegend, Clone: CD28.2, 1 µg/mL) for 72 hours. Next, CD8 T Cells were rested and expanded in fresh Immunocult media in the presence of 100 U/mL of human IL-2 (Peprotech) for a further 72 hours. Cells were then re-stimulated with plate bound anti-CD3 (Biolegend, Clone: OKT3 1 µg/mL) and anti-CD28 (Biolegend Clone: CD28.2 1 µg/mL) in the presence of 100 nM of cortisol [hydrocortisone (HC) – Sigma] or vehicle control (methanol, Sigma) for 48 hours. All procedures were approved by the Human Biology Research Ethics Committee of the University of Cambridge (HBREC2019.15).

CRISPR-Cas9 mediated *NR3C1* deletion

Seventy-two hours after T cell activation, cells were washed with PBS and resuspended in complete P3 Primary Cell Nucleofection Solution (Lonza) according to the manufacturer's instructions. For each nucleofection, 1×10^6 cells were used. Two distinct ribonucleoprotein (RNP) complexes were prepared, each targeting a specific sgRNA designed for the deletion of NR3C1. The sequences for the sgRNAs were as follows:

1. sgRNA 1: 5' – CUUUAAGUCUGUUUCCCCCG – 3'
2. sgRNA 2: 5'– AACCUCCAACAGUGACACCA – 3'

Both sgRNAs were synthesised by Synthego, and the Alt-R S.p. High Fidelity Cas9 Nuclease V3 (Integrated DNA Technologies) was used to form the RNP complexes. Each RNP complex was assembled at a 3:1 molar ratio of sgRNA to Cas9 (2.48 µM Cas9 + 7.52 µM sgRNA). The prepared Cas9 RNP complexes were mixed with the cells and transferred to a 20 µL Nucleocuvette Vessel. Electroporation was performed using a 4D Nucleofector with the EO-115 program (Lonza). For control experiments, NR3C1-sufficient CD8 T cells were processed in parallel and electroporated with High Fidelity Cas9 protein only (Mock Control). Immediately following nucleofection, 80 µL of pre-warmed ImmunoCult-XF media (without supplements) was added directly to the Nucleocuvette Vessel, and the cells were allowed to recover at 37°C for 20 minutes. The cells were then transferred to a 24-well plate and cultured for 72 hours in fresh ImmunoCult-XF media supplemented with 100 U/mL of IL-2 (PeproTech) and 50 µg/mL of Gentamicin (Gibco™).

Single-cell RNA sequencing (scRNA-seq), clustering and visualisation

The previously published and publicly available scRNA-seq datasets used in this study were as follows GSE164690[40-42], GSE161529[43,44], GSE127465[45], GSE155698[46,47] and an integrated scRNA seq of NSCLC from 103 patients[48]. The data has been downloaded from NCBI GEO (https://www.ncbi.nlm.nih.gov/geo/) and processed with the standard scRNA-seq integration pipeline in Seurat. To cluster the cells, we first identified the top 2,000 most variable genes using the FindVariableFeatures function in Seurat. For cell visualization, we applied the Uniform Manifold Approximation and Projection (UMAP) algorithm to project the cells' PCA space representation into two dimensions. Cell clustering in PCA space was performed with the Shared Nearest Neighbor (SNN) algorithm, using Seurat V3's FindNeighbors and FindClusters functions. We then visualised the resulting clusters in UMAP space with the DimPlot function. The differentially expressed genes in each cluster were identified with the FindAllMarkers function in Seurat. The clusters have been identified either by previous annotation or based on the Cluster Identity Predictor (CIPR) program and has been validated based on marker gene expression from Panglo DB. Gene expression levels were visualised using heatmaps, violin plots, and bar plots, created with the pheatmap package (version 1.0.12) (available at https://cran.r-project.org/web/packages/pheatmap) and the dittoSeq R package (version 1.2.4). Data scaling during visualization was performed automatically using the default settings of these packages. Cell type information was retrieved from the metadata slot of the downloaded object. To quantify GR-RUNX3 co-expression within tumour-infiltrating CD8 T Cells, we calculated the co-expression score as the geometric mean of log-normalised counts in single cell expression of *NR3C1* and *RUNX3*. Gene module scores for subpopulations, as defined above, were calculated using the Seurat function AddModuleScore. CD8 T-cell transcriptional states were quantified in a Seurat object using gene-signature module scoring.

Marker gene sets for CD8 T-cell states

Curated marker genes were compiled a priori to represent major CD8 T-cell states. The "general" marker sets comprised:

Naïve-like: *TCF7, CCR7, SELL, LEF1, IL7R, LTB*

Pre-dysfunctional: *GZMK, ZNF683, CD28, FYN, EOMES, CXCR3, CXCR4, CD44*

Dysfunctional/exhausted: *PDCD1, HAVCR2, LAG3, TIGIT, CTLA4, LAYN, CXCL13, ENTPD1, ITGAE, IFNG*

Cytotoxic: *CX3CR1, PRF1, GZMA, GZMB, GZMH, GNLY, FGFBP2, NKG7, KLRD1, FCGR3A, KLRG1*

Marker-gene expression and module scores were visualised on UMAP embeddings using FeaturePlot.

516

517 **Single-cell trajectory analysis**

518 Single-cell trajectory analysis was performed using Monocle (version 2.20.0). Briefly, size
519 factors and dispersions were estimated with default settings. Differentially expressed genes
520 were identified using Monocle's differentialGeneTest function (q-value < 0.01). Identified
521 genes were used as ordering genes. Dimensionality was reduced using the DDRTree
522 algorithm, and trajectories were constructed by ordering cells based on pseudotime.

523

524 **Western blot analysis**

525 72 hours post nucleofection, CD8 T cells were washed once with ice cold PBS and lysed in
526 radioimmunoprecipitation assay (RIPA) buffer (Merck) with proteinase and phosphatase
527 inhibitors (Roche). Protein concentrations were determined by Pierce™ BCA Protein Assay
528 Kit and performed according to the manufacturer's instructions (Thermo-Scientific). Protein
529 samples (15 µg) were separated on a NuPAGE 4-12% Bis-Tris polyacrylamide gels
530 (Invitrogen), transferred onto nitrocellulose membranes (Bio-Rad) and probed using rabbit
531 anti-GR (Clone: D6H2L, Cell Signaling Technology) and mouse beta-actin (Clone: 8H10,
532 Origene) antibodies. Detection of immunoreactive bands was performed using secondary goat
533 anti-rabbit IRDye™ 680CW and goat anti-mouse IRDye™ 800CW antibodies. Images
534 acquired on the Odyssey DLx imaging system (Li-COR).

535

536

537 **Bulk RNA sequencing analysis**

538 Cell pellets were layered with 40 µL of RNAlater Stabilization solution (Invitrogen) and stored
539 at -80°C prior to RNA extraction. Samples were homogenised using the QIAshredder Kit
540 (Qiagen) according to manufacturer's instructions. Next, total RNA was extracted using the
541 RNeasy Plus Mini Kit (Qiagen). RNA sequencing was performed in paired-end on Illumina
542 NovaSeq 6000 platform, yielding 40 million reads per sample (Novogene, UK). Raw
543 sequencing reads were quality-controlled with FastQC (version 0.11.9), followed by alignment
544 to the reference genome gencode version 42 (Homo sapiens genome hg38/GRCh38) using
545 the alignment tool hisat2 (version 2.2.1). The sam files were further inspected, filtered, and
546 processed using samtools (version 1.13). HTseq counts obtained from bam files were
547 annotated and subjected to DESeq2 (version 1.34.0) analysis in R (version 4.1.1). For DEseq2
548 analysis, for each gene, a log2 fold change was computed and the significance level was
549 assessed using the Wald test statistic with a p value and an adjusted p value. Differentially
550 expressed genes across different conditions have been identified using the cutoff of a p-
551 adjusted value of 0.05. The volcano plot has been constructed in GraphPad Prism 9.5.1 based
552 on the differentially expressed genes found in bulk RNA sequencing. After differential

553 expression analysis, genes were ranked according to their fold change and by using the
554 fGSEA algorithm, we performed Gene Set Enrichment Analysis (GSEA). The human collection
555 H (hallmark gene sets) from the Molecular Signatures Database (MSigDB) were used to
556 identify positively and negatively enriched pathways. All steps were performed in R version
557 4.1.1.
558
559 **Chromatin immunoprecipitation (ChIP) followed by sequencing**
560 Chromatin immunoprecipitation (ChIP) was performed using the SimpleChIP Enzymatic
561 Chromatin IP Kit (Cell Signaling Technology) following the manufacturer's protocol with minor
562 modifications. Briefly, cells were crosslinked with 1% formaldehyde (Merck) in serum-free
563 RPMI-1640 for 10 min at room temperature (RT) and quenched with 1X glycine for 5 min.
564 Nuclei were isolated and chromatin digested with 0.3 µL micrococcal nuclease in 200 µL ChIP
565 Buffer at 37 °C for 20 min, followed by brief sonication (Branson 450-D sonicator, amplitude
566 36%, 4 × 5 s pulses on ice). Chromatin was immunoprecipitated overnight at 4 °C with 1 µg
567 each of anti-GR antibodies (PA1-511A, Thermo-Scientific; D6H2L, Cell Signaling
568 Technology). Immune complexes were captured with ChIP-Grade Protein G Magnetic Beads
569 (2 h, 4 °C), washed sequentially with low-salt and high-salt buffers, and eluted with 1X ChIP
570 Elution Buffer at 65 °C for 30 min. Crosslinks were reversed at 65 °C for 2 hours (5 M NaCl,
571 Proteinase K), with DNA purified and submitted for Illumina sequencing (Novogene,
572 Cambridge, UK).
573
574 **ChIP-seq data analysis**
575 Raw reads from fastq files were first trimmed using fastp 0.20.0 with the setting '-l 25 --
576 detect_adapter_for_pe'. Trimmed reads were mapped to the human genome hg38 by hisat2
577 2.1.0 with default setting and sorted by samtools 1.9 with flag '-ShuF 4 -q 30 -f 2'. After
578 mapping, duplicated reads were removed by the picard tool (v.2.20.8)
579 (http://broadinstitute.github.io/picard/). Peaks were then called using MACS2 and annotated
580 using HOMER[49].
581
582 **Integration of bulk RNA-seq and ChIP-seq data**
583 After analysing bulk RNA-Seq and ChIP-Seq data, we compared the differentially expressed
584 genes in RNA-seq of cortisol treated vs. vehicle control and all annotated peaks in ChIP-seq
585 data. Downstream analysis was performed based on the genes between the RNA-seq and
586 HC-treated ChIP-seq peaks, which include a total of 35 genes. The venn diagram to visualise
587 the common genes was constructed using InteractiVenn. A heatmap has been drawn in gplots
588 (version 3.1.3) in R version 4.1.1 to show the normalised counts of genes (transformed into
589 row z-score) common in differentially expressed genes in RNA-seq and annotated peaks from

590 cortisol (HC) treated cells. The protein-protein interaction (PPI) network has been constructed
591 in STRING (version 11.5) and visualised in cytoscape (version 3.91). All 35 differentially
592 expressed genes have been used as inputs in STRING, but only 8 genes constitute an intact
593 network. The pie chart demonstrating the genomic position diversity of peaks obtained from
594 cortisol treated cells in ChIP-seq data has been constructed in GraphPad Prism 9.5.1.
595
596 **Overexpression of NR3C1 and RUNX3 in HEK-293T**
597 A custom polycistronic plasmid (EF1A > hRUNX3 [NM_001320672.1] : IRES : hNR3C1
598 [NM_001364185.1] : IRES : EGFP) was designed and generated by VectorBuilder. Driven by
599 the EF1A promoter, this construct produces a single mRNA transcript translated into RUNX3,
600 NR3C1 , and EGFP via IRES elements. HEK-293T cells were transfected with 5 µg of plasmid
601 using Lipofectamine 3000 (Invitrogen) in serum-free Opti-MEM, following the manufacturer's
602 protocol. Transfection was performed at 70–80% confluence. After 6 hours, 100nM of cortisol
603 (Sigma-Aldrich) was added directly to the culture medium, and cells were incubated for an
604 additional 48 hours to allow for cortisol-mediated effects.
605
606 **Co-Immunoprecipitation (Co-IP)**
607 Cells were harvested by washing with ice-cold PBS and collected by centrifugation at 300 × g
608 for 5 minutes at 4 °C. Cell lysis was performed using Pierce IP Lysis Buffer (Thermo Scientific)
609 supplemented with protease and PhosSTOP phosphatase inhibitors (Roche). Lysates were
610 incubated on ice for 30 minutes, followed by mild sonication (three 5 s pulses at 36%
611 amplitude) using a Branson 4D Sonicator. Lysates were cleared by centrifugation at
612 16,000 × g for 20 minutes at 4 °C. The supernatant was pre-cleared by incubation with 10 µL
613 of Protein A/G Plus-Agarose Beads (Santa Cruz) for 1 hour at 4 °C with rotation, followed by
614 centrifugation at 3,000 × g for 10 minutes. Clarified lysates were incubated overnight at 4 °C
615 with either anti-NR3C1 (D6H2L, Cell Signaling Technology; 1:100) or control rabbit IgG (Cell
616 Signaling Technology), followed by addition of 30 µL Protein A/G Plus-Agarose Beads and
617 further incubation for 2 hours at 4 °C. Beads were washed three times with lysis buffer, and
618 bound proteins were eluted in Laemmli sample buffer. Eluates were analysed by western
619 blotting using anti-RUNX1/AML1, RUNX3, and RUNX2 antibodies (EPR3099, Abcam). The
620 details of the mutations (ΔAF1-NR3C1, ΔTAD-RUNX3, ΔTAD ID-RUNX3) has been provided
621 in the supplementary document.
622
623 **Resource availability**
624 **Lead contact**
625 Further information and requests for resources and reagents should be directed to and will be
626 fulfilled by the Lead Contact, Bidesh Mahata (bm562@cam.ac.uk)

Material availability

This study did not generate unique reagents.

Data and code availability

- Data: Newly generated bulk RNA seq and ChIP seq data are deposited to EBI ArrayExpress with the accession numbers E-MTAB-16594, E-MTAB-16635 (https://www.ebi.ac.uk/biostudies/arrayexpress).
- Code: This paper does not report original code.
- Additional information: Any additional information required to reanalyse the data reported in this paper is available from the lead contact upon request.

Author contribution

CJW, SC, SKS, AAD, CVV, QZ, JP, XC and BM performed the experiments, analysed, interpreted & visualised the data. BM conceptualised and supervised the study. All authors read and approved the draft manuscript before submission.

Acknowledgements

We would like to thank Dr Andrew Conway-Morris, University of Cambridge for providing ethical support; Amit Mandal, University of Oxford, for critical suggestion and advice on RNA-seq data analysis. We used BioRender.com to generate the graphical illustrations presented in this manuscript.

Funding

The work is supported by CRUK Career Development Fellowship (RCCFEL\100095), NSF-BIO/UKRI-BBSRC project grant (BB/V006126/1) and MRC project grant (MR/V028995/1).

Competing interests

The authors declare that they have no competing interests.

Data and materials availability

All newly generated data such as RNA sequencing and ChIP sequencing data used in the study will be available in the public database during revised submission stage.

Supplementary tables

661 Supplementary Table S1: Cortisol-induced genes in human CD8 T cell

662 Supplementary Table S2: Cortisol-induced hallmark pathways in CD8 T cell

663 Supplementary Table S3: Glucocorticoid binding peaks in CD8 T cell

664 Supplementary Table S4: Glucocorticoid direct target genes in CD8 T cell

665 Supplementary Table S5: Cortisol induced genes, ChIP-seq peaks, RUNX regulated genes
666
667 **References**
668

669 1. Cain, D.W., and Cidlowski, J.A. (2017). Immune regulation by glucocorticoids. Nat Rev
670 Immunol *17*, 233-247. 10.1038/nri.2017.1.
671 2. Vandewalle, J., Luypaert, A., De Bosscher, K., and Libert, C. (2018). Therapeutic
672 Mechanisms of Glucocorticoids. Trends Endocrinol Metab *29*, 42-54.
673 10.1016/j.tem.2017.10.010.
674 3. Quatrini, L., and Ugolini, S. (2021). New insights into the cell- and tissue-specificity of
675 glucocorticoid actions. Cell Mol Immunol *18*, 269-278. 10.1038/s41423-020-00526-2.
676 4. Obradovic, M.M.S., Hamelin, B., Manevski, N., Couto, J.P., Sethi, A., Coissieux, M.M.,
677 Munst, S., Okamoto, R., Kohler, H., Schmidt, A., and Bentires-Alj, M. (2019).
678 Glucocorticoids promote breast cancer metastasis. Nature *567*, 540-544.
679 10.1038/s41586-019-1019-4.
680 5. Acharya, N., Madi, A., Zhang, H., Klapholz, M., Escobar, G., Dulberg, S., Christian, E.,
681 Ferreira, M., Dixon, K.O., Fell, G., et al. (2020). Endogenous Glucocorticoid Signaling
682 Regulates CD8(+) T Cell Differentiation and Development of Dysfunction in the Tumor
683 Microenvironment. Immunity *53*, 658-671 e656. 10.1016/j.immuni.2020.08.005.
684 6. Mahata, B., Pramanik, J., van der Weyden, L., Polanski, K., Kar, G., Riedel, A., Chen, X.,
685 Fonseca, N.A., Kundu, K., Campos, L.S., et al. (2020). Tumors induce de novo steroid
686 biosynthesis in T cells to evade immunity. Nat Commun *11*, 3588. 10.1038/s41467-
687 020-17339-6.
688 7. Chakraborty, S., Pramanik, J., and Mahata, B. (2021). Revisiting steroidogenesis and its
689 role in immune regulation with the advanced tools and technologies. Genes Immun
690 *22*, 125-140. 10.1038/s41435-021-00139-3.
691 8. Pramanik, J., Shaji, S.K., Zaman, M., Brown, B., Zhang, B., Yamashita-Kanemaru, Y.,
692 Homer, N.Z.M., Hussein, H.A.M., Zhao, Q., Okkenhaug, K., et al. (2025). Drug
693 repurposing reveals posaconazole as a CYP11A1 inhibitor enhancing anti-tumor
694 immunity. iScience *28*, 112488. 10.1016/j.isci.2025.112488.
695 9. Zhao, Q., Pramanik, J., Lu, Y., Homer, N.Z.M., Imianowski, C.J., Zhang, B., Iqbal, M.,
696 Shaji, S.K., Morris, A.C., Roychoudhuri, R., et al. (2025). Perturbing local
697 steroidogenesis to improve breast cancer immunity. Nat Commun *16*, 3945.
698 10.1038/s41467-025-59356-3.
699 10. Sandor, L.F., Huh, J.B., Benko, P., Hiraga, T., Poliska, S., Dobo-Nagy, C., Simpson, J.P.,
700 Homer, N.Z.M., Mahata, B., and Gyori, D.S. (2024). De novo steroidogenesis in tumor
701 cells drives bone metastasis and osteoclastogenesis. Cell Rep *43*, 113936.
702 10.1016/j.celrep.2024.113936.
703 11. Weikum, E.R., Knuesel, M.T., Ortlund, E.A., and Yamamoto, K.R. (2017). Glucocorticoid
704 receptor control of transcription: precision and plasticity via allostery. Nat Rev Mol
705 Cell Biol *18*, 159-174. 10.1038/nrm.2016.152.

706 12. De Bosscher, K., Beck, I.M., Dejager, L., Bougarne, N., Gaigneaux, A., Chateauvieux, S.,
707 Ratman, D., Bracke, M., Tavernier, J., Vanden Berghe, W., et al. (2014). Selective
708 modulation of the glucocorticoid receptor can distinguish between transrepression of
709 NF-kappaB and AP-1. Cell Mol Life Sci *71*, 143-163. 10.1007/s00018-013-1367-4.
710 13. Escoter-Torres, L., Greulich, F., Quagliarini, F., Wierer, M., and Uhlenhaut, N.H. (2020).
711 Anti-inflammatory functions of the glucocorticoid receptor require DNA binding.
712 Nucleic Acids Res *48*, 8393-8407. 10.1093/nar/gkaa565.
713 14. Franco, L.M., Gadkari, M., Howe, K.N., Sun, J., Kardava, L., Kumar, P., Kumari, S., Hu,
714 Z., Fraser, I.D.C., Moir, S., et al. (2019). Immune regulation by glucocorticoids can be
715 linked to cell type-dependent transcriptional responses. J Exp Med *216*, 384-406.
716 10.1084/jem.20180595.
717 15. Wherry, E.J., and Kurachi, M. (2015). Molecular and cellular insights into T cell
718 exhaustion. Nat Rev Immunol *15*, 486-499. 10.1038/nri3862.
719 16. Philip, M., and Schietinger, A. (2022). CD8(+) T cell differentiation and dysfunction in
720 cancer. Nat Rev Immunol *22*, 209-223. 10.1038/s41577-021-00574-3.
721 17. Giles, A.J., Hutchinson, M.N.D., Sonnemann, H.M., Jung, J., Fecci, P.E., Ratnam, N.M.,
722 Zhang, W., Song, H., Bailey, R., Davis, D., et al. (2018). Dexamethasone-induced
723 immunosuppression: mechanisms and implications for immunotherapy. J
724 Immunother Cancer *6*, 51. 10.1186/s40425-018-0371-5.
725 18. Xia, M., Gasser, J., and Feige, U. (1999). Dexamethasone enhances CTLA-4 expression
726 during T cell activation. Cell Mol Life Sci *55*, 1649-1656. 10.1007/s000180050403.
727 19. Seo, W., and Taniuchi, I. (2020). The Roles of RUNX Family Proteins in Development of
728 Immune Cells. Mol Cells *43*, 107-113. 10.14348/molcells.2019.0291.
729 20. Mevel, R., Draper, J.E., Lie, A.L.M., Kouskoff, V., and Lacaud, G. (2019). RUNX
730 transcription factors: orchestrators of development. Development *146*.
731 10.1242/dev.148296.
732 21. Korinfskaya, S., Parameswaran, S., Weirauch, M.T., and Barski, A. (2021). Runx
733 Transcription Factors in T Cells-What Is Beyond Thymic Development? Front Immunol
734 *12*, 701924. 10.3389/fimmu.2021.701924.
735 22. Woolf, E., Xiao, C., Fainaru, O., Lotem, J., Rosen, D., Negreanu, V., Bernstein, Y.,
736 Goldenberg, D., Brenner, O., Berke, G., et al. (2003). Runx3 and Runx1 are required for
737 CD8 T cell development during thymopoiesis. Proc Natl Acad Sci U S A *100*, 7731-7736.
738 10.1073/pnas.1232420100.
739 23. Milner, J.J., Toma, C., Yu, B., Zhang, K., Omilusik, K., Phan, A.T., Wang, D., Getzler, A.J.,
740 Nguyen, T., Crotty, S., et al. (2017). Runx3 programs CD8(+) T cell residency in non-
741 lymphoid tissues and tumours. Nature *552*, 253-257. 10.1038/nature24993.
742 24. Egawa, T., Tillman, R.E., Naoe, Y., Taniuchi, I., and Littman, D.R. (2007). The role of the
743 Runx transcription factors in thymocyte differentiation and in homeostasis of naive T
744 cells. J Exp Med *204*, 1945-1957. 10.1084/jem.20070133.
745 25. Lu, L., Wen, Y., Yao, Y., Chen, F., Wang, G., Wu, F., Wu, J., Narayanan, P., Redell, M.,
746 Mo, Q., and Song, Y. (2018). Glucocorticoids Inhibit Oncogenic RUNX1-ETO in Acute
747 Myeloid Leukemia with Chromosome Translocation t(8;21). Theranostics *8*, 2189-
748 2201. 10.7150/thno.22800.
749 26. Khan, S.H., Ling, J., and Kumar, R. (2011). TBP binding-induced folding of the
750 glucocorticoid receptor AF1 domain facilitates its interaction with steroid receptor
751 coactivator-1. PLoS One *6*, e21939. 10.1371/journal.pone.0021939.

752 27. van der Leun, A.M., Thommen, D.S., and Schumacher, T.N. (2020). CD8(+) T cell states
753 in human cancer: insights from single-cell analysis. Nat Rev Cancer *20*, 218-232.
754 10.1038/s41568-019-0235-4.
755 28. Taves, M.D., and Ashwell, J.D. (2021). Glucocorticoids in T cell development,
756 differentiation and function. Nat Rev Immunol *21*, 233-243. 10.1038/s41577-020-
757 00464-0.
758 29. Shimba, A., Cui, G., Tani-Ichi, S., Ogawa, M., Abe, S., Okazaki, F., Kitano, S., Miyachi,
759 H., Yamada, H., Hara, T., et al. (2018). Glucocorticoids Drive Diurnal Oscillations in T
760 Cell Distribution and Responses by Inducing Interleukin-7 Receptor and CXCR4.
761 Immunity *48*, 286-298 e286. 10.1016/j.immuni.2018.01.004.
762 30. Hong, J.Y., Lim, J., Carvalho, F., Cho, J.Y., Vaidyanathan, B., Yu, S., Annicelli, C., Ip,
763 W.K.E., and Medzhitov, R. (2020). Long-Term Programming of CD8 T Cell Immunity by
764 Perinatal Exposure to Glucocorticoids. Cell *180*, 847-861 e815.
765 10.1016/j.cell.2020.02.018.
766 31. John, S., Sabo, P.J., Thurman, R.E., Sung, M.H., Biddie, S.C., Johnson, T.A., Hager, G.L.,
767 and Stamatoyannopoulos, J.A. (2011). Chromatin accessibility pre-determines
768 glucocorticoid receptor binding patterns. Nat Genet *43*, 264-268. 10.1038/ng.759.
769 32. Stavreva, D.A., Coulon, A., Baek, S., Sung, M.H., John, S., Stixova, L., Tesikova, M.,
770 Hakim, O., Miranda, T., Hawkins, M., et al. (2015). Dynamics of chromatin accessibility
771 and long-range interactions in response to glucocorticoid pulsing. Genome Res *25*,
772 845-857. 10.1101/gr.184168.114.
773 33. Voss, T.C., and Hager, G.L. (2014). Dynamic regulation of transcriptional states by
774 chromatin and transcription factors. Nat Rev Genet *15*, 69-81. 10.1038/nrg3623.
775 34. Biddie, S.C., John, S., Sabo, P.J., Thurman, R.E., Johnson, T.A., Schiltz, R.L., Miranda,
776 T.B., Sung, M.H., Trump, S., Lightman, S.L., et al. (2011). Transcription factor AP1
777 potentiates chromatin accessibility and glucocorticoid receptor binding. Mol Cell *43*,
778 145-155. 10.1016/j.molcel.2011.06.016.
779 35. Ahmed, A., Reinhold, C., Breunig, E., Phan, T.S., Dietrich, L., Kostadinova, F., Urwyler,
780 C., Merk, V.M., Noti, M., Toja da Silva, I., et al. (2023). Immune escape of colorectal
781 tumours via local LRH-1/Cyp11b1-mediated synthesis of immunosuppressive
782 glucocorticoids. Mol Oncol *17*, 1545-1566. 10.1002/1878-0261.13414.
783 36. Michalek, S., Goj, T., Plazzo, A.P., Marovca, B., Bornhauser, B., and Brunner, T. (2022).
784 LRH-1/NR5A2 interacts with the glucocorticoid receptor to regulate glucocorticoid
785 resistance. EMBO Rep *23*, e54195. 10.15252/embr.202154195.
786 37. Taves, M.D., Otsuka, S., Taylor, M.A., Donahue, K.M., Meyer, T.J., Cam, M.C., and
787 Ashwell, J.D. (2023). Tumors produce glucocorticoids by metabolite recycling, not
788 synthesis, and activate Tregs to promote growth. J Clin Invest *133*. 10.1172/JCI164599.
789 38. Merk, V.M., Grob, L., Fleischmann, A., and Brunner, T. (2023). Human lung carcinomas
790 synthesize immunoregulatory glucocorticoids. Genes Immun *24*, 52-56.
791 10.1038/s41435-023-00194-y.
792 39. Sidler, D., Renzulli, P., Schnoz, C., Berger, B., Schneider-Jakob, S., Fluck, C., Inderbitzin,
793 D., Corazza, N., Candinas, D., and Brunner, T. (2011). Colon cancer cells produce
794 immunoregulatory glucocorticoids. Oncogene *30*, 2411-2419. 10.1038/onc.2010.629.
795 40. Kurten, C.H.L., Kulkarni, A., Cillo, A.R., Santos, P.M., Roble, A.K., Onkar, S., Reeder, C.,
796 Lang, S., Chen, X., Duvvuri, U., et al. (2021). Investigating immune and non-immune
797 cell interactions in head and neck tumors by single-cell RNA sequencing. Nat Commun
798 *12*, 7338. 10.1038/s41467-021-27619-4.

41. Janjic, B.M., Kulkarni, A., Ferris, R.L., Vujanovic, L., and Vujanovic, N.L. (2022). Human B Cells Mediate Innate Anti-Cancer Cytotoxicity Through Concurrent Engagement of Multiple TNF Superfamily Ligands. Front Immunol *13*, 837842. 10.3389/fimmu.2022.837842.
42. Wang, J., Li, H., Kulkarni, A., Anderson, J.L., Upadhyay, P., Onyekachi, O.V., Arantes, L., Banerjee, H., Kane, L.P., Zhang, X., et al. (2025). Differential impact of TIM-3 ligands on NK cell function. J Immunother Cancer *13*. 10.1136/jitc-2024-010618.
43. Pal, B., Chen, Y., Vaillant, F., Capaldo, B.D., Joyce, R., Song, X., Bryant, V.L., Penington, J.S., Di Stefano, L., Tubau Ribera, N., et al. (2021). A single-cell RNA expression atlas of normal, preneoplastic and tumorigenic states in the human breast. EMBO J *40*, e107333. 10.15252/embj.2020107333.
44. Chen, Y., Pal, B., Lindeman, G.J., Visvader, J.E., and Smyth, G.K. (2022). R code and downstream analysis objects for the scRNA-seq atlas of normal and tumorigenic human breast tissue. Sci Data *9*, 96. 10.1038/s41597-022-01236-2.
45. Zilionis, R., Engblom, C., Pfirschke, C., Savova, V., Zemmour, D., Saatcioglu, H.D., Krishnan, I., Maroni, G., Meyerovitz, C.V., Kerwin, C.M., et al. (2019). Single-Cell Transcriptomics of Human and Mouse Lung Cancers Reveals Conserved Myeloid Populations across Individuals and Species. Immunity *50*, 1317-1334 e1310. 10.1016/j.immuni.2019.03.009.
46. Steele, N.G., Carpenter, E.S., Kemp, S.B., Sirihorachai, V.R., The, S., Delrosario, L., Lazarus, J., Amir, E.D., Gunchick, V., Espinoza, C., et al. (2020). Multimodal Mapping of the Tumor and Peripheral Blood Immune Landscape in Human Pancreatic Cancer. Nat Cancer *1*, 1097-1112. 10.1038/s43018-020-00121-4.
47. Halbrook, C.J., Thurston, G., Boyer, S., Anaraki, C., Jimenez, J.A., McCarthy, A., Steele, N.G., Kerk, S.A., Hong, H.S., Lin, L., et al. (2022). Differential integrated stress response and asparagine production drive symbiosis and therapy resistance of pancreatic adenocarcinoma cells. Nat Cancer *3*, 1386-1403. 10.1038/s43018-022-00463-1.
48. Prazanowska, K.H., and Lim, S.B. (2023). An integrated single-cell transcriptomic dataset for non-small cell lung cancer. Sci Data *10*, 167. 10.1038/s41597-023-02074-6.
49. Pramanik, J., Chen, X., Kar, G., Henriksson, J., Gomes, T., Park, J.E., Natarajan, K., Meyer, K.B., Miao, Z., McKenzie, A.N.J., et al. (2018). Genome-wide analyses reveal the IRE1a-XBP1 pathway promotes T helper cell differentiation by resolving secretory stress and accelerating proliferation. Genome Med *10*, 76. 10.1186/s13073-018-0589-3.

Figure legends

Figure 1. Genome-wide effect of glucocorticoid signalling in activated CD8 T cell

- **a.** Schematic flowchart of the experimental strategy used to identify glucocorticoid-regulated genes in human CD8 T cells. CD8 T cells from three healthy donors were purified, activated, and expanded. *NR3C1* (encoding glucocorticoid receptor) was deleted in half of the cells. Wild type and GR-knockout CD8 T cells were then reactivated in the presence or absence of physiological levels (100 nM) of cortisol for 48 hours, to comprehensively identify glucocorticoid-dependent gene expression changes in CD8 T cells by RNA-seq.
  Specification of the samples (b-g): KO denotes GR knockout, Mock denotes wildtype, HC denotes hydrocortisone (cortisol) treated. Veh denotes vehicle.
- **b.** Volcano plot depicting the differentially expressed genes in human primary activated CD8 T cells after cortisol treatment. The significantly upregulated genes have been shown in red and the significantly downregulated genes have been shown in blue. log2-Fold change versus –log10(adjusted p-value) has been plotted, n = 3 human samples in each group.
- **c.** The hallmark biological processes associated with cortisol-treated CD8 T cells. Prognosis-ranked gene set enrichment analysis (GSEA) identified hallmark pathways that are differentially regulated. Normalised enrichment scores (NES) were calculated for all 50 hallmark pathways in GSEA. Upregulated (shown in red) and downregulated (shown in blue) gene sets are displayed, with their NES values represented on the x-axis.
- **d.** Knockout (KO) of glucocorticoid receptor encoding gene *NR3C1* in CD8 T cells using CRISPR-Cas9 targeting exon 2 and exon 5 (top panel). The knockout efficiency has been validated by western blot (bottom panel).
- **e.** Volcano plot showing the differentially expressed genes in *NR3C1* KO activated CD8 T cells compared to mock activated CD8 T cells, in the presence of cortisol.
- **f.** The intersections in Venn diagrams showing the cortisol-induced GR-dependent upregulated and downregulated genes.
- **g.** Expression heatmap showing the cortisol-induced transcription factors and receptors (transcription factor, cytokine receptor, transporters, cell surface and adhesion receptor) from differentially expressed genes (log2FC> 1, log2FC <-1 and p.adj < 0.05).

Figure 2. Genome-wide chromatin binding of GR identifies non-canonical transcription factor binding motif in CD8 T cells

a. Diagrammatic flowchart of the experimental strategy. CD8 T cells from healthy donors were purified, activated and propagated. Resting CD8 T cells were reactivated the presence or absence of physiological level (100 nM) cortisol to find out genome-wide chromatin binding of GR by ChIP-seq.

b. Homer motif analysis of cortisol-treated CD8 T cells. The top 4 enriched GR binding peaks and corresponding motifs have been shown for two healthy donors (HC-A & HC-B) in cortisol-treated CD8 T Cells. The motifs have been arranged in descending order of abundance/enrichment. For each motif, the best match transcription factor and percentage of GR peaks containing the motif are indicated. HC-A & HC-B: Hydrocortisone (HC)/cortisol-treated donor-A & donor-B samples.

c. Venn diagram showing the common number of peaks between hydrocortisone (cortisol) treated CD8 T cells from two donors.

d. Venn diagram showing glucocorticoid (GC)-induced peaks comparing vehicle-treated and cortisol (HC)-treated CD8 T cells.

e. The Venn diagram shows the direct targets of glucocorticoids after intersecting GR binding peaks from ChIP-seq data and cortisol-induced upregulated genes.

f. The Venn diagram shows all GR-RUNX co-regulated genes that are also direct targets of GR.

g. Genome browser tracks showing GR ChIP-seq signal in activated CD8 T cells from three independent healthy donors (donor A-C) treated with vehicle or hydrocortisone (HC). The glucocorticoid-influenced and GR-RUNX-regulated four genes are shown here. The shaded region highlights the cortisol-induced GR peaks with the predicted RUNX motif annotated above the peaks. DNase I hypersensitivity signal is shown as an indicator of chromatin accessibility.

Figure 3. RUNX3 transcription factor cooperate with the glucocorticoid receptor to regulate gene expression

a. Schematic illustration of the experimental strategy (left). HEK 293T cells were transfected with GR and RUNX3 expressing plasmid construct. Cell lysates were immunoprecipitated by using anti-GR antibody and immunoblotted by RUNX antibody. Representative immunoblot shown in the right panel.

b. Domain architecture of GR (NR3C1) and RUNX3, and the deletions used to map the interaction interface. For GR, the N-terminal AF-1 (NTD) region was deleted (ΔAF1-NR3C1). For RUNX3, the C-terminal transactivation/inhibition region was deleted (ΔTAD-RUNX3 and ΔTAD-ID-RUNX3).

c. Co-IP mapping of the GR–RUNX3 interaction interface. Anti-GR (NR3C1) co-immunoprecipitation was performed in HEK-293T cells expressing wild-type (WT) GR and RUNX3 or the indicated deletion mutants (ΔAF1-NR3C1, ΔTAD-RUNX3, ΔTAD/ID-RUNX3). To assess ligand dependence, HEK-293T cells co-expressing WT GR and RUNX3 were treated with cortisol (+) or vehicle (–) prior to anti-GR co-IP. Input and immunoprecipitated fractions were immunoblotted with anti-RUNX3 and anti-GR (NR3C1) antibodies.

d. Venn diagrams showing the GR-RUNX3 co-regulated genes by integrating cortisol induced genes (upregulated and downregulated), all GR binding peaks from ChIP-seq, GR binding site containing RUNX motif and RUNX3 target genes. The corresponding heatmap showing the expression of GR-RUNX3 co-regulated genes in vehicle-treated CD8 T cells, cortisol (hydrocortisone or HC) treated CD8 T cell and *NR3C1* KO CD8 T cells.

Figure 4. Single-cell transcriptomics study reveals the expression of cortisol responder genes in different tumour-infiltrating CD8 T cells

a-d. UMAP-based clustering of scRNA-seq data was used to identify CD8 T cell populations from tumour and matched blood or normal tissue samples in breast cancer (**a**), lung cancer (**b**), head and neck squamous cell carcinoma (HNSC) (**c**), and pancreatic ductal adenocarcinoma (PDAC) (**d**). Dot plots show the proportion of cells (dot size) and the average expression (colour intensity) of selected top cortisol responder genes within tumour-infiltrating CD8 T cells and corresponding peripheral blood or matched tissue-resident CD8 T cells. The data highlight distinct patterns of steroid-responsive gene expression between tumour-infiltrating and non-tumour CD8 T cell populations, reflecting the influence of the tumour microenvironment on CD8 T cell transcriptional states and potential links to T cell dysfunction and immune evasion

Figure 5. RUNX and GR co-regulated gene expression in tumour-infiltrating CD8 T cells across cancer types

a–d, Single-cell transcriptomic profiling of CD8 T cells isolated from tumours and matched non-tumour compartments (matched blood or matched non-cancerous tissue) in triple-negative breast cancer (TNBC) (a), lung cancer (b), head and neck squamous cell carcinoma (HNSC) (c), and pancreatic ductal adenocarcinoma (PDAC) (d). Top, UMAP feature plots showing the distribution of CD8 T cells (blue) with *NR3C1* (GR) and *RUNX3* expression (colour scale; grey indicates low/absent signal, red indicates higher expression). Bottom, dot plots summarising expression of the RUNX–GR co-regulated gene set across tumour-infiltrating

CD8 T cells and matched non-tumour CD8 T cells (TNBC: adjacent tissue; lung/HNSC/PDAC: blood). Dot plots show expression of the RUNX–GR co-regulated gene set (a 50-gene core signature defined by integrating GR–RUNX1-, GR–RUNX2- and GR–RUNX3-mediated upregulated gene sets. Dot size indicates the fraction of cells expressing each gene and colour intensity denotes average expression. Across all tumour types, RUNX–GR co-regulated genes are expressed at higher levels in tumour-infiltrating CD8 T cells compared with their non-tumour counterparts **.**

e-h. To assess the functional relevance of RUNX and GR co-regulated gene expression, module scores were calculated using the AddModuleScore method for each CD8 T cell. High module scores, indicative of elevated co-regulated gene expression, were associated with increased expression of exhaustion-related genes, highlighting a link between RUNX2/GR transcriptional activity and the exhausted phenotype in tumour-infiltrating CD8 T cells across TNBC **(e)**, lung cancer **(f)**, HNSC **(g)**, and PDAC **(h)**.

Figure 6. GR–RUNX co-regulated gene expression is enriched in pre-dysfunctional tumour-infiltrating CD8 T cells across solid cancers

a–d, Feature plots showing module scores for naïve-like, cytotoxic, dysfunctional and pre-dysfunctional CD8 T cell transcriptional states, together with the GR–RUNX co-regulated gene module in tumour-infiltrating CD8 T cells from **a,** triple-negative breast cancer (TNBC), **b,** lung cancer, **c,** head and neck squamous cell carcinoma (HNSC) and **d,** pancreatic ductal adenocarcinoma (PDAC). Colour intensity indicates relative module score (higher scores shown in darker red). Across tumour types, cytotoxic CD8 T cells make distinct cluster from GR–RUNX module–expressing CD8 T cells, whereas GR–RUNX module activity preferentially localises to areas enriched for the pre-dysfunctional programme and adjacent to dysfunctional states.

Supplementary Figure S1. Comparative *RUNX 1, 2* and *3* expression and identification of GR-RUNX 1 and 2 co-regulated genes

- **a.** Genomic distribution of GR binding sites in HC-treated CD8 T cells.
- **b.** Comparative *RUNX 1, 2* and *3* expression in activated CD8 T cells in the RNAseq. Normalised expression of these genes from different donors has been plotted here
- **c.** Venn diagram depicting the set of genes jointly regulated by the GR and RUNX1, identified through an integrative analysis of cortisol-induced upregulated genes, GR ChIP-seq peaks, GR peaks containing RUNX1 motifs, and known RUNX1 target genes. Expression levels of the overlapping gene set are visualised in a heatmap across multiple experimental conditions.

d. Venn diagram illustrating the genes co-regulated by GR and RUNX2, identified by integrating cortisol-responsive genes (both upregulated and downregulated), GR ChIP-seq data, GR peaks with RUNX2 motifs, and annotated RUNX2 targets. Expression patterns of these shared genes under different conditions are shown in the accompanying heatmap. Specification of the samples: KO denotes glucocorticoid receptor (GR) knockout, HC denotes hydrocortisone (cortisol) treated. Mock denotes wildtype. Veh denotes vehicle.

Supplementary Figure S2. Single-cell trajectory analysis of CD8 T cells from lung tumours and blood samples

a. Pseudo-temporal trajectories of CD8 T cells inferred using Monocle, coloured by sample origin and pseudotime.

b. Expression patterns of cortisol-responsive genes (*TSC22D3, IL7R, FKBP5*) and inhibitory receptors (*PDCD1, CTLA4, HAVCR2, TIGIT, LAYN, TOX*) along the inferred trajectories.

Supplementary Figure S3. Original western blots

a. This western blot corresponds to Figure 1d.

b. These western blots correspond to Figure 3c.

Figure 1

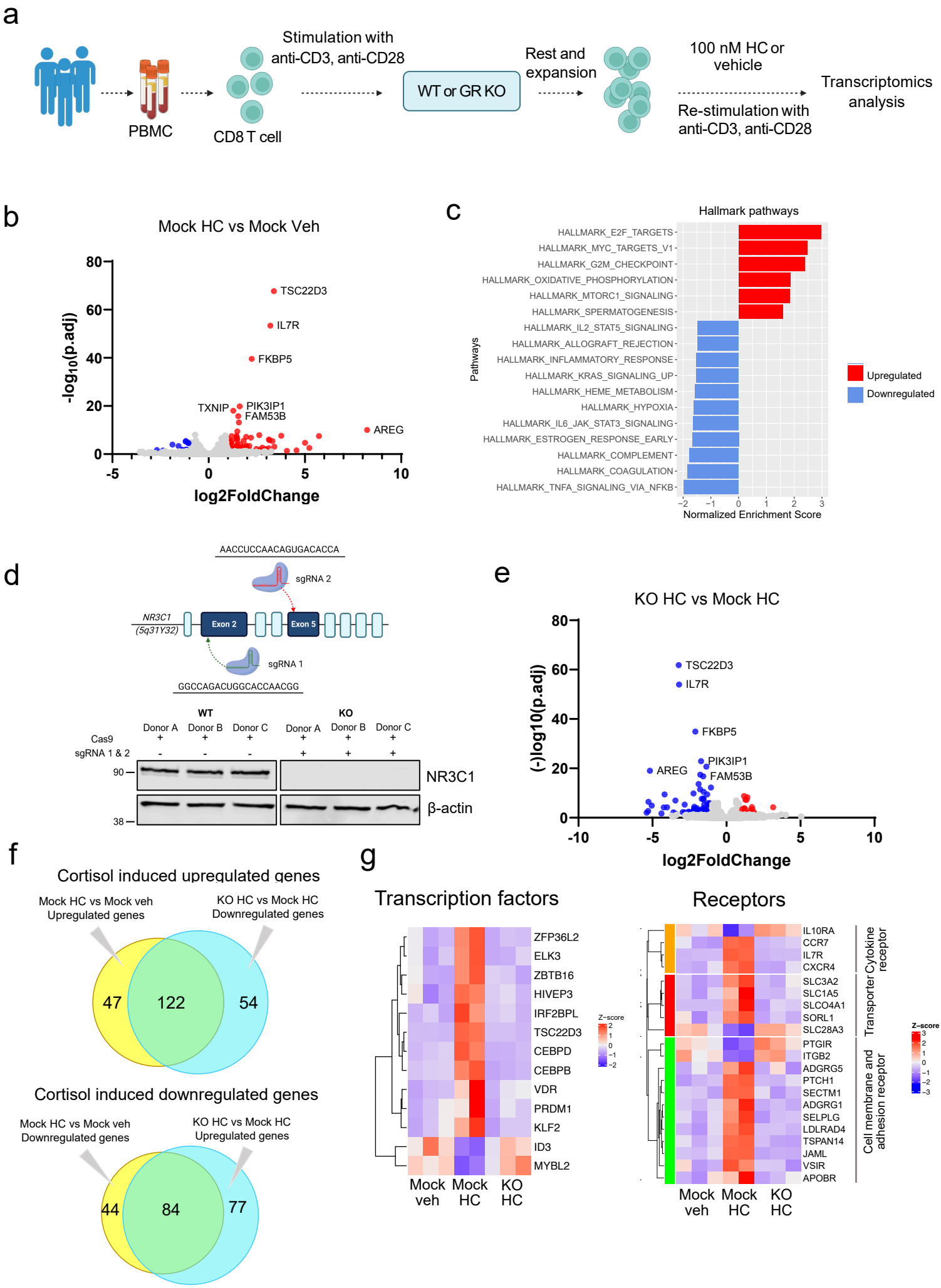
a
PBMC
CD8 T cell
Stimulation with anti-CD3, anti-CD28
WT or GR KO
Rest and expansion
100 nM HC or vehicle
Re-stimulation with anti-CD3, anti-CD28
Transcriptomics analysis
b
Mock HC vs Mock Veh
-log10(p.adj)
log2FoldChange
TSC22D3
IL7R
FKBP5
TXNIP
PIK3IP1
FAM53B
AREG
c
Hallmark pathways
Pathways
HALLMARK_E2F_TARGETS
HALLMARK_MYC_TARGETS_V1
HALLMARK_G2M_CHECKPOINT
HALLMARK_OXIDATIVE_PHOSPHORYLATION
HALLMARK_MTORC1_SIGNALING
HALLMARK_SPERMATOGENESIS
HALLMARK_IL2_STAT5_SIGNALING
HALLMARK_ALLOGRAFT_REJECTION
HALLMARK_INFLAMMATORY_RESPONSE
HALLMARK_KRAS_SIGNALING_UP
HALLMARK_HEME_METABOLISM
HALLMARK_HYPOXIA
HALLMARK_IL6_JAK_STAT3_SIGNALING
HALLMARK_ESTROGEN_RESPONSE_EARLY
HALLMARK_COMPLEMENT
HALLMARK_COAGULATION
HALLMARK_TNFA_SIGNALING_VIA_NFKB
Normalized Enrichment Score
Upregulated
Downregulated
d
AACCUCCAACAGUGACACCA
sgRNA 2
NR3C1 (5q31Y32)
Exon 2
Exon 5
sgRNA 1
GGCCAGACUGGCACCAACGG
WT
KO
Donor A
Donor B
Donor C
Cas9
sgRNA 1 & 2
90
38
NR3C1
β-actin
e
KO HC vs Mock HC
(-)log10(p.adj)
log2FoldChange
TSC22D3
IL7R
FKBP5
PIK3IP1
FAM53B
AREG
f
Cortisol induced upregulated genes
Mock HC vs Mock veh Upregulated genes
KO HC vs Mock HC Downregulated genes
47
122
54
Cortisol induced downregulated genes
Mock HC vs Mock veh Downregulated genes
KO HC vs Mock HC Upregulated genes
44
84
77
g
Transcription factors
ZFP36L2
ELK3
ZBTB16
HIVEP3
IRF2BPL
TSC22D3
CEBPD
CEBPB
VDR
PRDM1
KLF2
ID3
MYBL2
Z-score
Mock veh
Mock HC
KO HC
Receptors
IL10RA
CCR7
IL7R
CXCR4
SLC3A2
SLC1A5
SLCO4A1
SORL1
SLC28A3
PTGIR
ITGB2
ADGRG5
PTCH1
SECTM1
ADGRG1
SELPLG
LDLRAD4
TSPAN14
JAML
VSIR
APOBR
Cytokine receptor
Transporter
Cell membrane and adhesion receptor
Z-score
Mock veh
Mock HC
KO HC

Figure 2

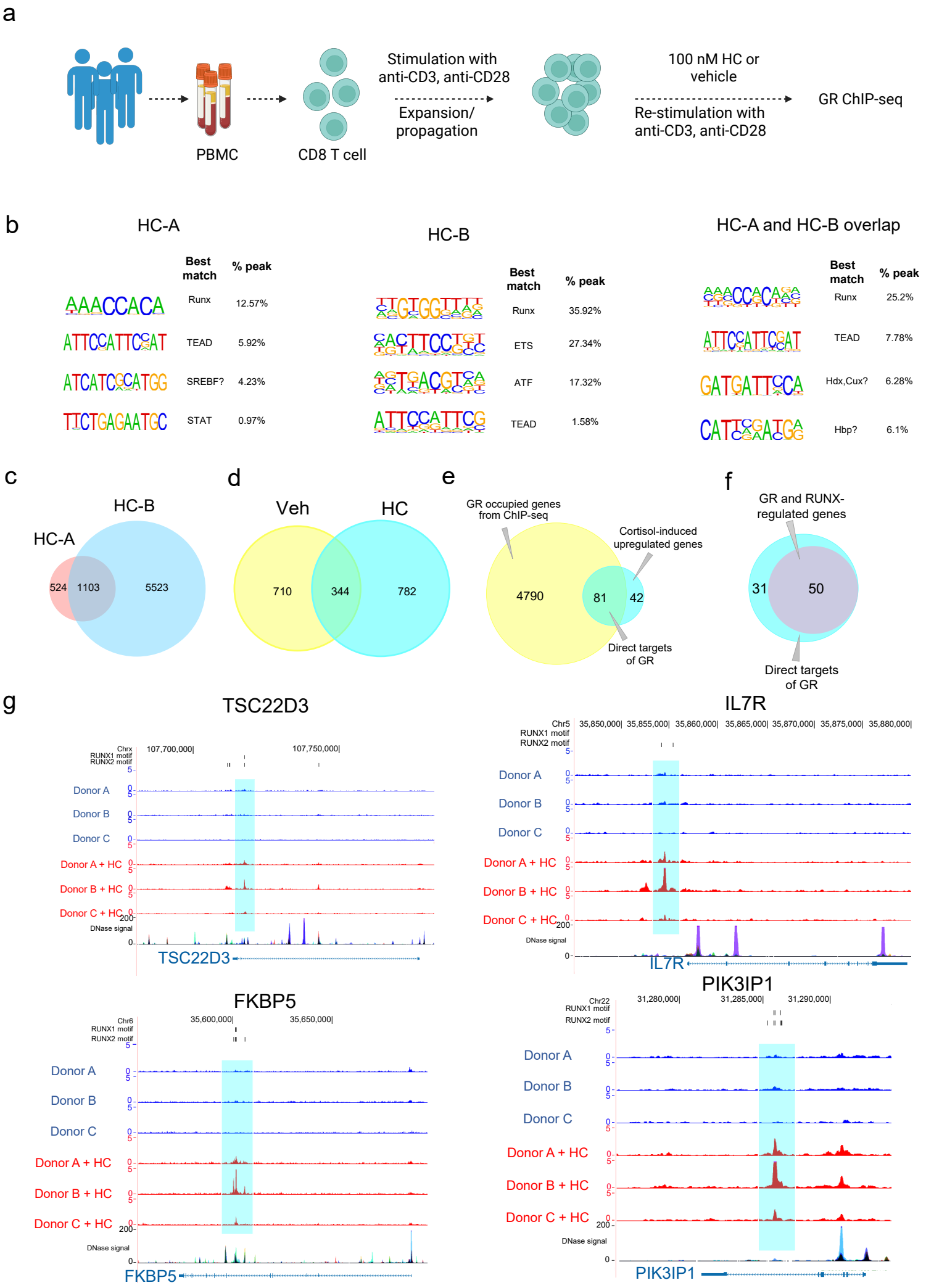
a
PBMC
CD8 T cell
Stimulation with anti-CD3, anti-CD28
Expansion/ propagation
100 nM HC or vehicle
Re-stimulation with anti-CD3, anti-CD28
GR ChIP-seq
b
HC-A
Best match
% peak
Runx 12.57%
TEAD 5.92%
SREBF? 4.23%
STAT 0.97%
HC-B
Best match
% peak
Runx 35.92%
ETS 27.34%
ATF 17.32%
TEAD 1.58%
HC-A and HC-B overlap
Best match
% peak
Runx 25.2%
TEAD 7.78%
Hdx,Cux? 6.28%
Hbp? 6.1%
c
HC-A
HC-B
524
1103
5523
d
Veh
HC
710
344
782
e
GR occupied genes from ChIP-seq
Cortisol-induced upregulated genes
4790
81
42
Direct targets of GR
f
GR and RUNX-regulated genes
31
50
Direct targets of GR
g
TSC22D3
Chrx
107,700,000
107,750,000
RUNX1 motif
RUNX2 motif
Donor A
Donor B
Donor C
Donor A + HC
Donor B + HC
Donor C + HC
DNase signal
TSC22D3
IL7R
Chr5
35,850,000
35,855,000
35,860,000
35,865,000
35,870,000
35,875,000
35,880,000
IL7R
FKBP5
Chr6
35,600,000
35,650,000
FKBP5
PIK3IP1
Chr22
31,280,000
31,285,000
31,290,000
PIK3IP1

Figure 3

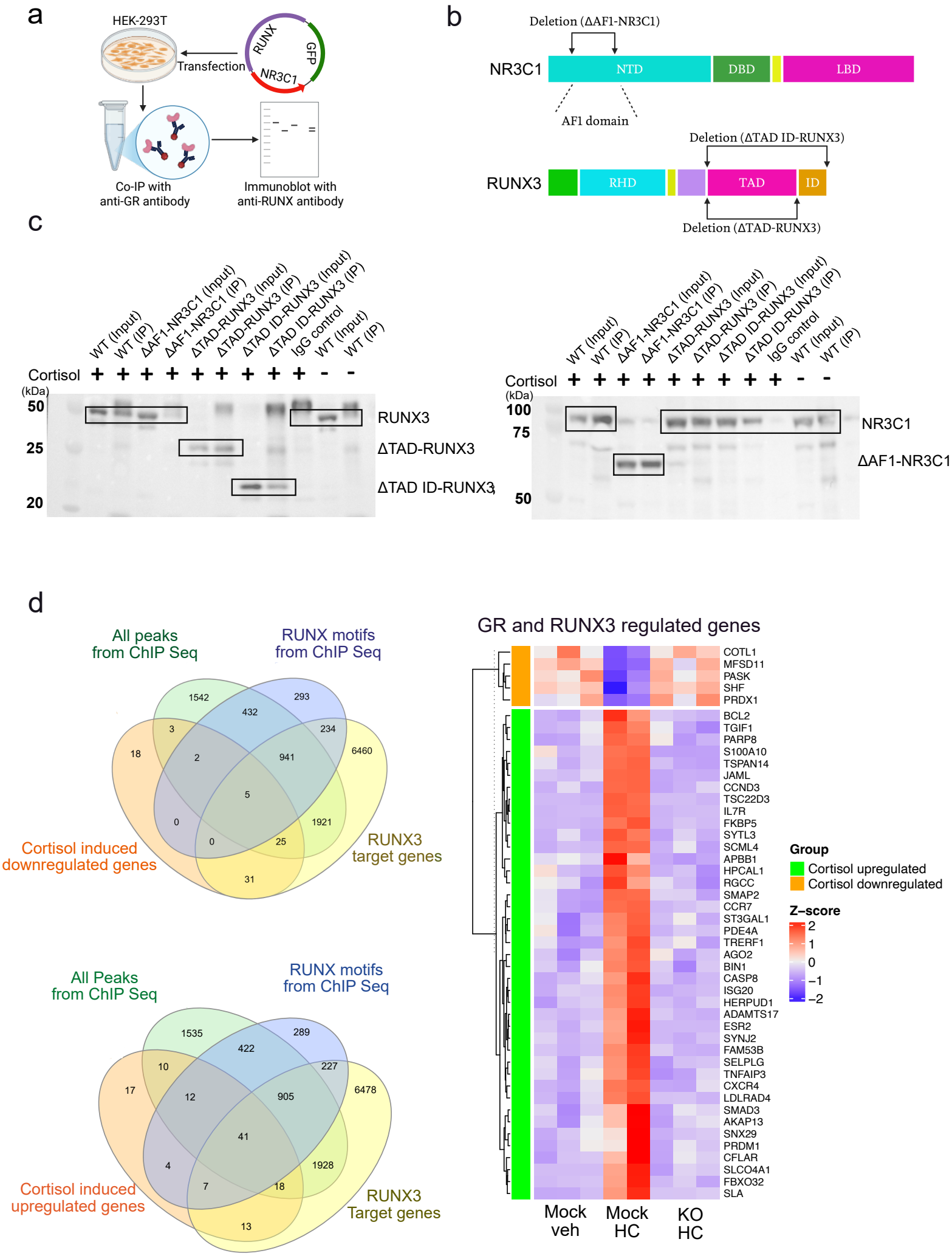
a
HEK-293T
Transfection
RUNX
GFP
NR3C1
Co-IP with
anti-GR antibody
Immunoblot with
anti-RUNX antibody
b
Deletion (ΔAF1-NR3C1)
NR3C1
NTD
DBD
LBD
AF1 domain
Deletion (ΔTAD ID-RUNX3)
RUNX3
RHD
TAD
ID
Deletion (ΔTAD-RUNX3)
c
WT (Input)
WT (IP)
ΔAF1-NR3C1 (Input)
ΔAF1-NR3C1 (IP)
ΔTAD-RUNX3 (Input)
ΔTAD-RUNX3 (IP)
ΔTAD ID-RUNX3 (Input)
ΔTAD ID-RUNX3 (IP)
IgG control
WT (Input)
WT (IP)
Cortisol
(kDa)
RUNX3
ΔTAD-RUNX3
ΔTAD ID-RUNX3
NR3C1
ΔAF1-NR3C1
d
All peaks
from ChIP Seq
RUNX motifs
from ChIP Seq
Cortisol induced
downregulated genes
RUNX3
target genes
All Peaks
from ChIP Seq
RUNX motifs
from ChIP Seq
Cortisol induced
upregulated genes
RUNX3
Target genes
GR and RUNX3 regulated genes
COTL1
MFSD11
PASK
SHF
PRDX1
BCL2
TGIF1
PARP8
S100A10
TSPAN14
JAML
CCND3
TSC22D3
IL7R
FKBP5
SYTL3
SCML4
APBB1
HPCAL1
RGCC
SMAP2
CCR7
ST3GAL1
PDE4A
TRERF1
AGO2
BIN1
CASP8
ISG20
HERPUD1
ADAMTS17
ESR2
SYNJ2
FAM53B
SELPLG
TNFAIP3
CXCR4
LDLRAD4
SMAD3
AKAP13
SNX29
PRDM1
CFLAR
SLCO4A1
FBXO32
SLA
Mock
veh
Mock
HC
KO
HC
Group
Cortisol upregulated
Cortisol downregulated
Z–score

Figure 4

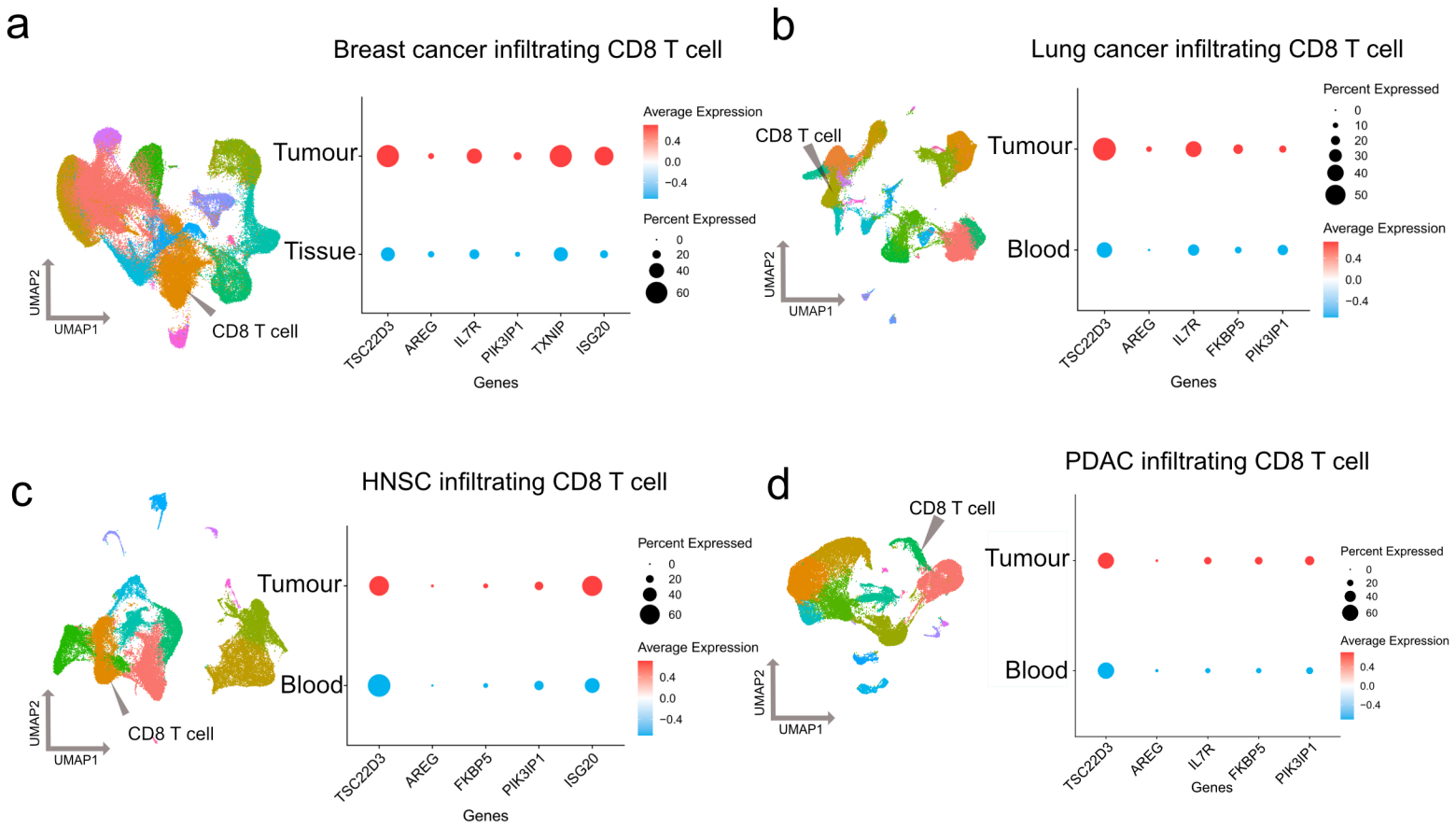
a
Breast cancer infiltrating CD8 T cell
Tumour
Tissue
CD8 T cell
UMAP2
UMAP1
Average Expression
0.4
0.0
−0.4
Percent Expressed
0
20
40
60
TSC22D3
AREG
IL7R
PIK3IP1
TXNIP
ISG20
Genes
b
Lung cancer infiltrating CD8 T cell
CD8 T cell
Tumour
Blood
Percent Expressed
0
10
20
30
40
50
Average Expression
0.4
0.0
−0.4
TSC22D3
AREG
IL7R
FKBP5
PIK3IP1
Genes
c
HNSC infiltrating CD8 T cell
Tumour
Blood
CD8 T cell
Percent Expressed
0
20
40
60
Average Expression
0.4
0.0
−0.4
TSC22D3
AREG
FKBP5
PIK3IP1
ISG20
Genes
d
PDAC infiltrating CD8 T cell
CD8 T cell
Tumour
Blood
Percent Expressed
0
20
40
60
Average Expression
0.4
0.0
−0.4
TSC22D3
AREG
IL7R
FKBP5
PIK3IP1
Genes

Figure 5

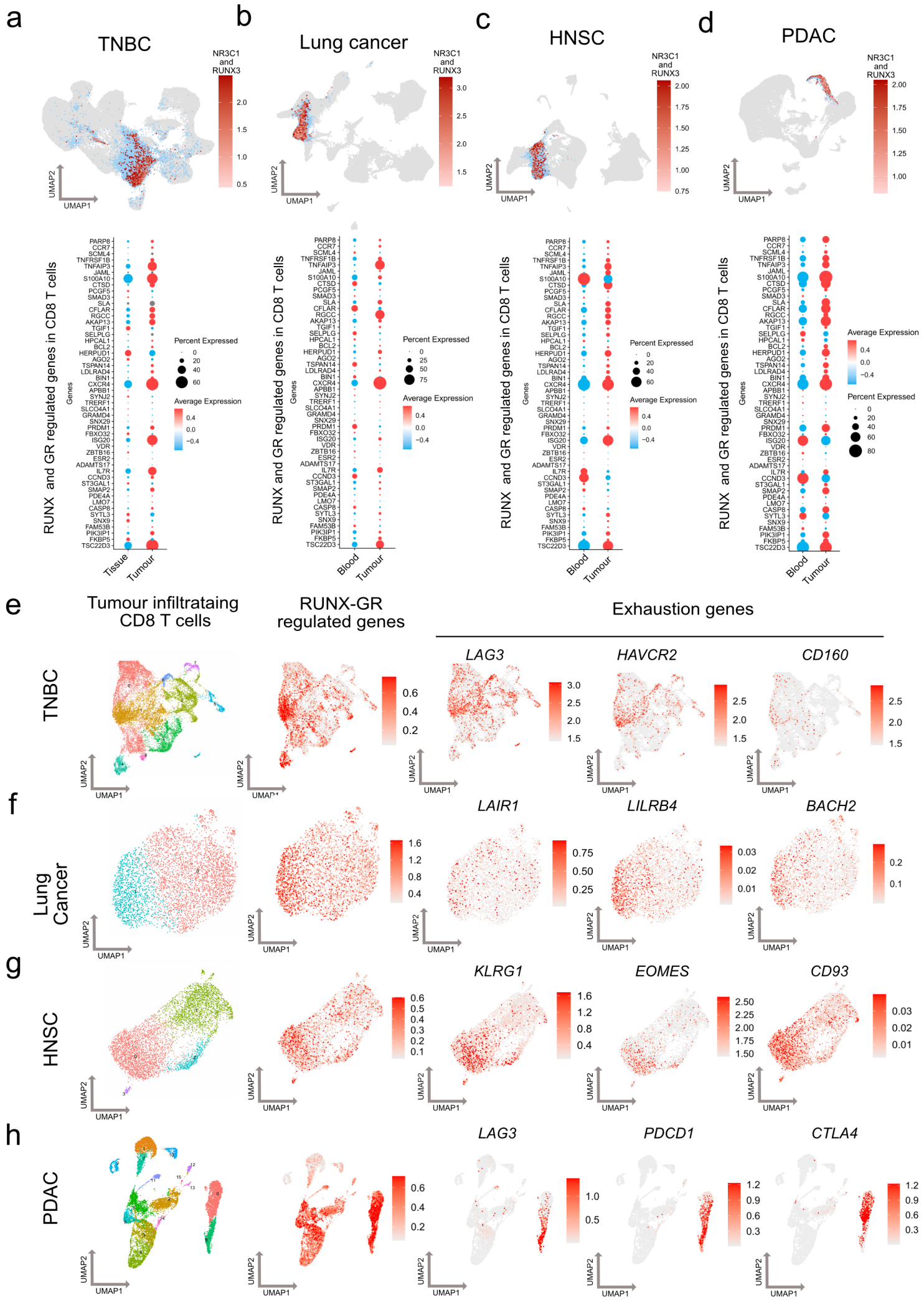
a
TNBC
b
Lung cancer
c
HNSC
d
PDAC
NR3C1 and RUNX3
UMAP1
UMAP2
RUNX and GR regulated genes in CD8 T cells
Genes
Tissue
Tumour
Blood
Percent Expressed
Average Expression
e
Tumour infiltrataing CD8 T cells
RUNX-GR regulated genes
Exhaustion genes
TNBC
LAG3
HAVCR2
CD160
f
Lung Cancer
LAIR1
LILRB4
BACH2
g
HNSC
KLRG1
EOMES
CD93
h
PDAC
LAG3
PDCD1
CTLA4

Figure 6

a

TNBC tumor-infiltrataing CD8T

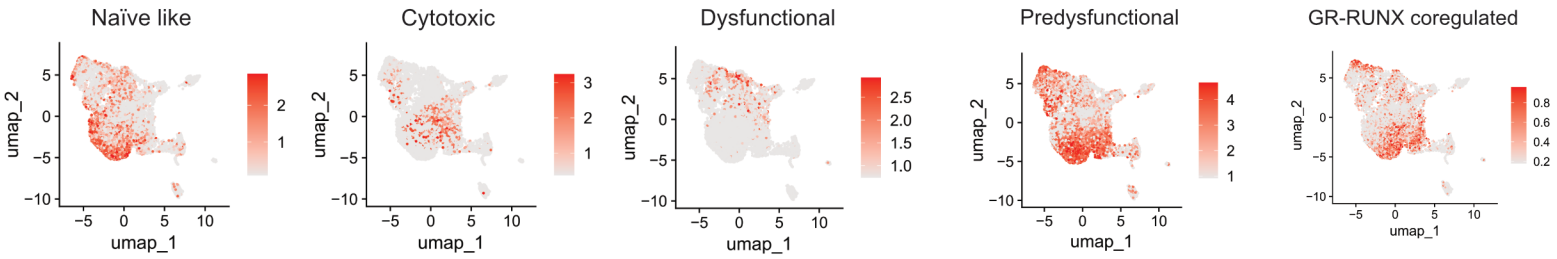

b

Lung tumor-infiltrataing CD8T

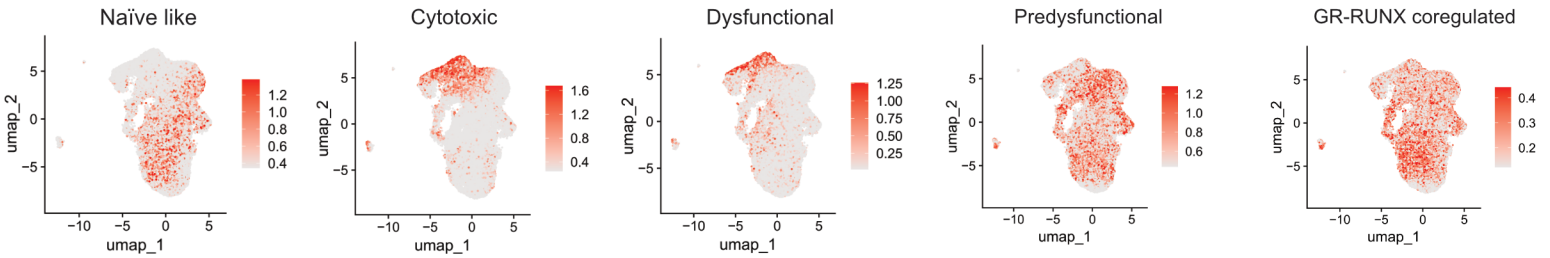

c

HNSC tumor-infiltrataing CD8T

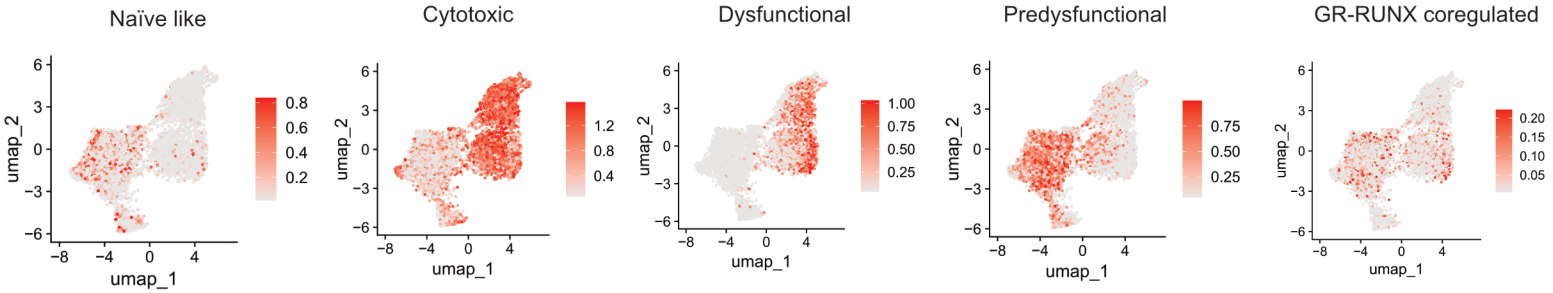

d

PDAC tumor-infiltrataing CD8T

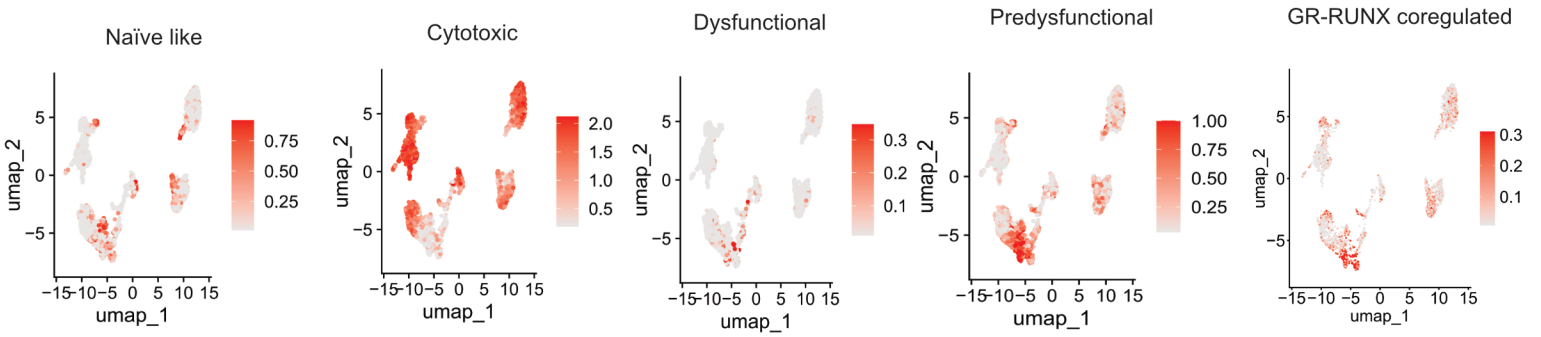

Supplementary Figure S1

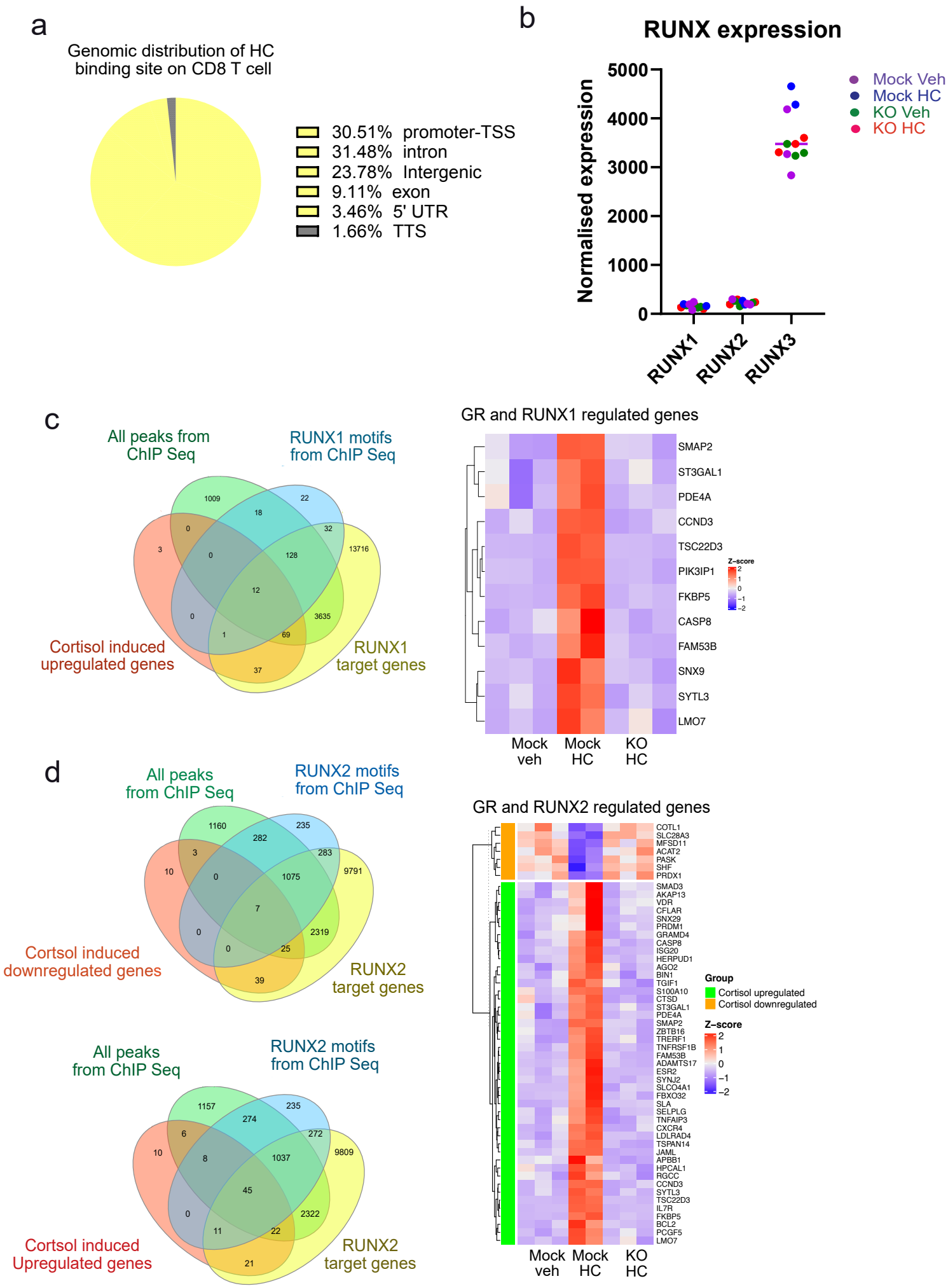

Supplementary Figure S2

a

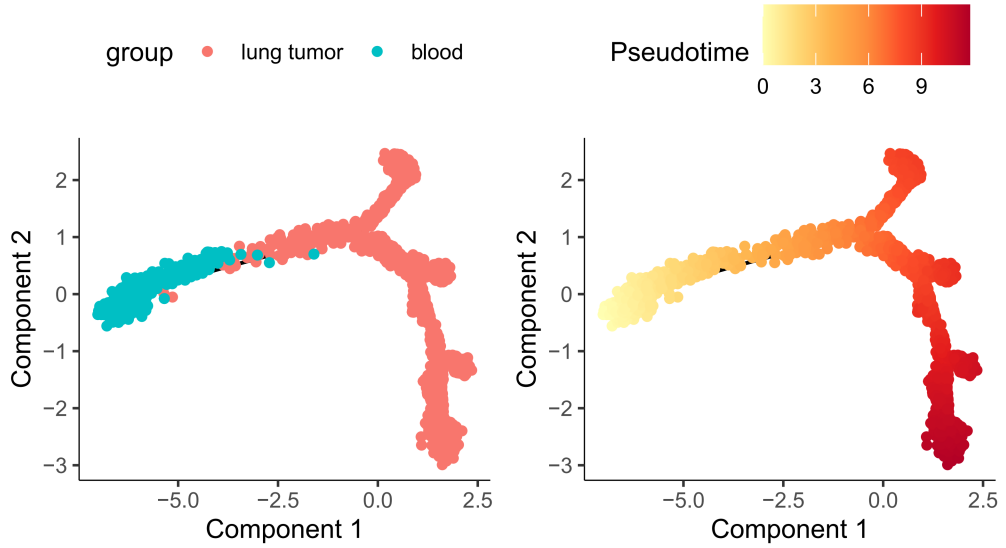

b

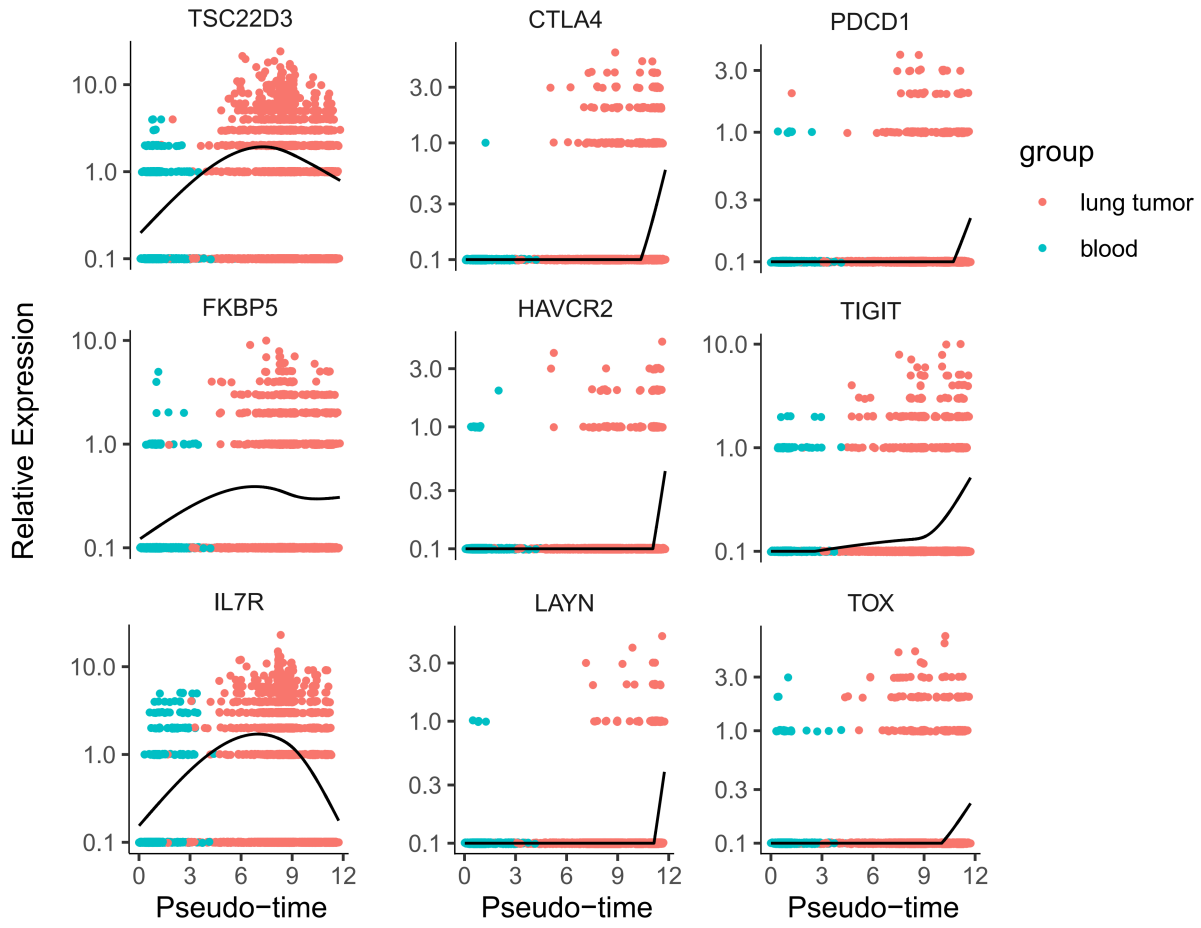

Supplementary figure S3

a

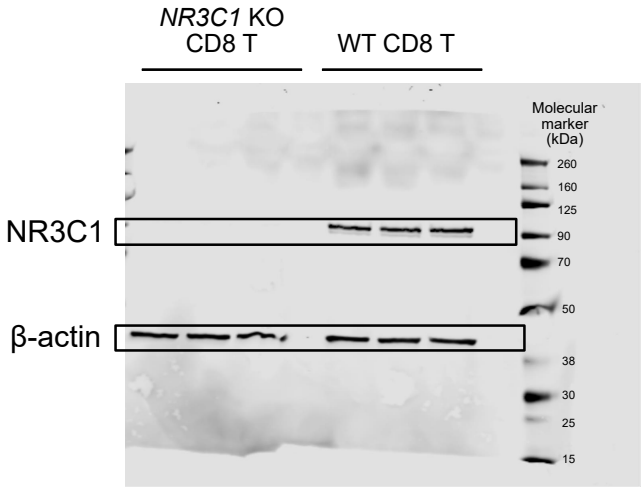
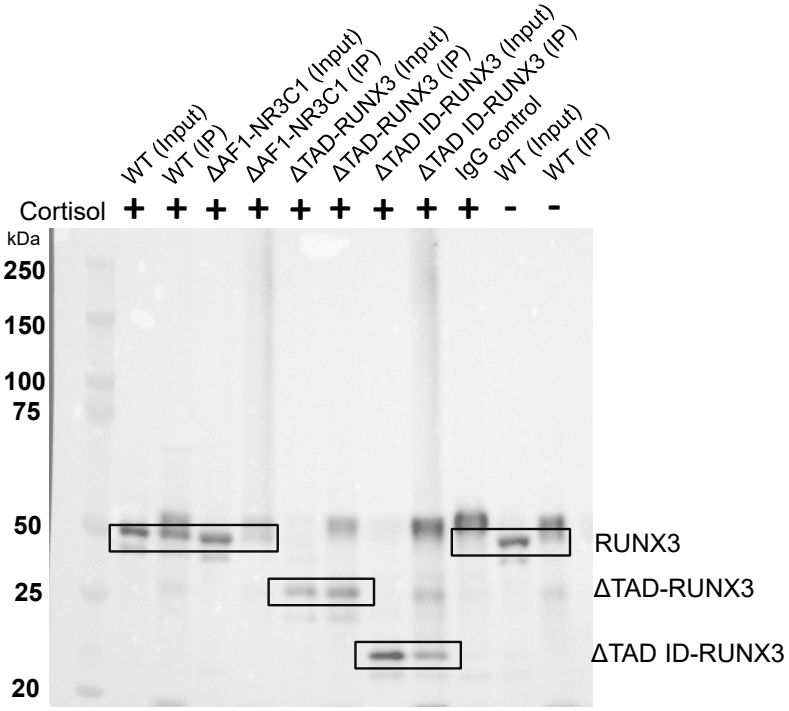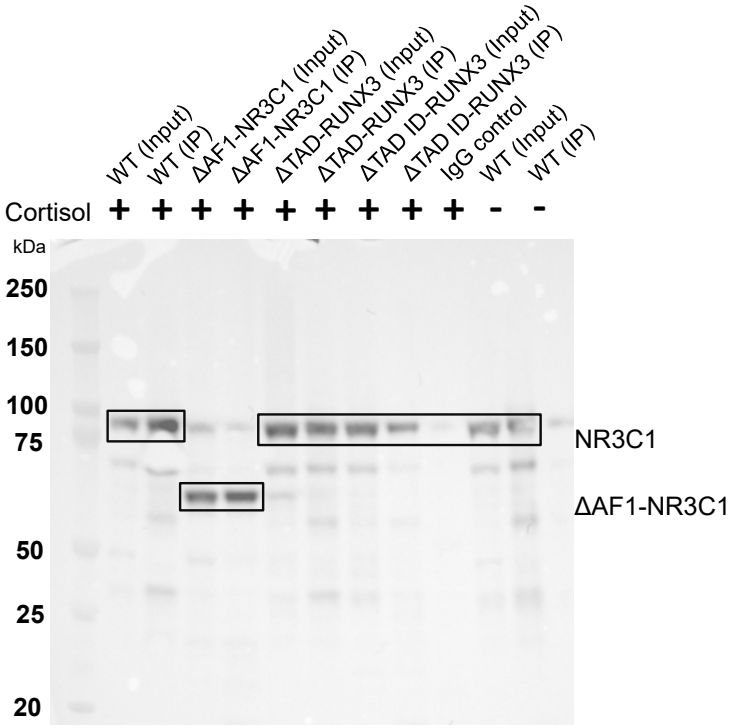
b